A Potential Vorticity Diagnostic Approach to Upper-Level Frontogenesis within a Developing Baroclinic Wave

MATTHEW S. WANDISHIN* AND JOHN W. NIELSEN-GAMMON

Department of Atmospheric Sceinces, Texas A&M University, College Station, Texas

DANIEL KEYSER

Department of Earth and Atmospheric Sciences, The University at Albany, State University of New York, Albany, New York

(Manuscript received 15 March 1999, in final form 11 April 2000)

ABSTRACT

The process of tropopause folding is studied in the context of the life cycle of baroclinic waves. Previous studies of upper-level frontogenesis have emphasized the role of the vertical circulation in driving stratospheric air down into the midtroposphere. Here, a potential vorticity–based approach is adopted that focuses on the generation of a folded tropopause. To facilitate comparison of the two approaches, the diagnosis is applied to the upper-level front previously simulated and studied by Rotunno et al. The potential vorticity approach clarifies the primary role played by the horizontal nondivergent wind in producing a fold and explains why folding should be a common aspect of baroclinic development.

Between the trough and upstream ridge, prolonged subsidence within a region of weak system-relative flow generates a tropopause depression oriented at an angle to the large-scale flow. The large-scale vertical shear then locally increases the slope of the tropopause, eventually leading to a tropopause fold. In contrast, tropopause folding in the base of the trough is caused by the nondivergent cyclonic circulation associated with the surface thermal wave. The winds associated with the thermal wave amplify the potential vorticity wave aloft, and these winds, which decrease with height, rapidly generate a tropopause fold within the trough.

1. Introduction

In 1955, Reed documented a tropopause folding event in a study of upper-level fronts. In the 40 years since that study, tropopause folds have been shown to influence surface cyclogenesis (e.g., Uccellini et al. 1985), to be associated with clear-air turbulence (e.g., Shapiro 1981), to trigger heavy precipitation events (e.g., Uccellini and Kocin 1987), and to account for a large portion of the mass exchange from the stratosphere to the troposphere (e.g., Lamarque and Hess 1994). Still, while a good deal is known about the structure of tropopause folds and their relationship to other phenomena, there are still questions about the root causes of tropopause folds themselves, or the processes governing their formation and evolution in the context of larger-scale processes such as cyclogenesis. For example, to what extent and by what mechanisms does cyclogenesis itself promote the development of tropopause folds?

Previous work does not provide a clear answer to this question. Tropopause folds are known to be a common aspect of cyclogenesis. Studies of tropopause folds during cyclogenesis (Uccellini et al. 1985; Lackmann et al. 1997) have argued that pronounced folding precedes intense cyclogenesis. Other studies, both idealized (Whitaker et al. 1988; Hines and Mechoso 1991; Bush and Peltier 1994) and observational (Reed and Sanders 1953; Reed 1955; Staley 1960; Bosart 1970; Shapiro 1970), have studied tropopause folding during cyclogenesis but have not established a direct relationship between tropopause folding and cyclogenesis. On the other hand, it is well known that tropopause folding can occur in the absence of surface cyclogenesis (e.g., Sanders et al. 1991).

Many recent studies, beginning with Hoskins et al. (1985), have demonstrated the usefulness of understanding processes associated with cyclogenesis in terms of potential vorticity (PV). In particular, piecewise PV inversion (Davis 1992) has been used to understand the roles of upper-level and lower-level features in cyclogenesis (e.g., Davis and Emanuel 1991; Davis et al.

* Current affiliation: Institute of Atmospheric Physics, The University of Arizona, Tucson, Arizona.

Corresponding author address: Matthew S. Wandishin, NSSL/NOAA, 1313 Halley Circle, Norman, OK 73069
E-mail: mwand@vicksburg.nssl.noaa.gov

1993) and in upper-level mobile trough evolution (Hakim et al. 1996; Nielsen-Gammon and Lefevre 1996). In this study, piecewise PV inversion will be used to investigate the role of an upper-level trough–jet system and a surface thermal wave in the development and intensification of a tropopause fold in a model of the life cycle of an idealized baroclinic wave. It will be shown that the intensifying cyclone in the model is configured such that the winds associated with the surface thermal wave will induce tropopause folding in the base of the upper-level trough.

The use of PV also suggests a fundamentally different way of viewing tropopause folds and upper-level fronts. In conventional kinematic studies, upper-level frontogenesis is defined in terms of the rate of change of the horizontal temperature gradient. Diagnosis focuses on the frontogenetical role of the ageostrophic vertical circulation and on the net effect on the temperature gradient of the geostrophic forcing and the ageostrophic response. The subsiding branch of the ageostrophic vertical circulation is viewed as producing the tropopause fold. However, in the PV perspective the upper-level front is manifested as a steep or folded tropopause, and frontogenesis consists of the quasi-two-dimensional, nearly isentropic advection and redistribution of PV into a folded structure, principally by the balanced winds attributable to the PV itself. This perspective yields new insights into the nature of tropopause folding and upper-level frontogenesis. For example, the transverse circulation is seen not as the cause of tropopause folding, but as the response needed to maintain thermal wind balance during PV redistribution.

A recent attempt to diagnose upper-level frontogenesis in terms of PV was made by Davies and Rossa (1998). However, in diagnosing the formation of PV signatures of upper-level fronts, they did not fully consider the dynamically relevant aspects of the PV distribution. For example, they diagnose the rate of change of the isentropic PV gradient, claiming that strong PV gradients on isentropic surfaces should imply enhanced baroclinicity above and below. However, a PV discontinuity can be present at the tropopause without necessarily implying enhanced baroclinicity. The seminal frontogenesis studies by Hoskins (1971, 1972) showed that an upper-level front and tropopause fold can evolve from initially weak baroclinicity in response to background deformation, with the PV remaining discontinuous throughout the evolution. The key PV feature for enhanced baroclinicity is not the presence of a strong gradient on a single isentropic surface, but the presence of a gradient throughout a layer spanning a range of isentropic surfaces. The development of such a deep feature—manifested as a vertical tropopause—is precisely the process diagnosed in the present paper.

In order to reconcile the PV approach with conventional methods, it is applied here to the investigation of a tropopause fold that was previously the subject of a comprehensive article by Rotunno et al. (1994, hereafter RSS). The folding takes place during an idealized baroclinic wave life cycle simulated using an adiabatic, inviscid channel model. The model and the study by RSS are summarized in section 2 in the context of historical issues regarding upper-level frontogenesis. Section 3 describes the methods for diagnosing folding, including the introduction of the ''foldogenesis function'' for quantifying the rate of change of the tropopause slope. The diagnostic results are presented in section 4, including quantitative evaluation of the roles of the nondivergent and irrotational winds [partitioned following Keyser et al. (1989) and Loughe et al. (1995)], as well as the nondivergent winds associated with the upper- and lower-level PV distributions [partitioned following Davis and Emanuel (1991)]. The results are summarized in section 5.

2. Background

a. Previous studies

The transverse ageostrophic circulation, particularly the descending branch, has been a topic of considerable interest in the history of research on upper-level fronts. The differential subsidence in the descending branch is seen as the primary mechanism for producing upper-level fronts. Idealized modeling studies by Hoskins and Bretherton (1972) showed this transverse circulation to be of a thermally direct sense, supporting the theory first proposed by Namias and Clapp (1949). However, one would expect the vertical motion pattern associated with a direct circulation to be frontolytical, and, indeed, observations by Reed and Sanders (1953), Staley (1960), Shapiro (1970), Bosart (1970), and others indicated that the vertical motion patterns were of a thermally indirect sense in intensifying upper-level fronts. This apparent contradiction was resolved by Keyser and Pecnick (1985) and Reeder and Keyser (1988) using a generalization of the two-dimensional frontogenesis problem formulated by Hoskins and Bretherton (1972). Confirming a hypothesis proposed by Shapiro (1981), Keyser and Pecnick (1985) and Reeder and Keyser (1988) found that when the thermal gradient possesses a component in the alongfront direction such as to produce cold advection, this mechanism, in addition to geostrophic confluence, strengthens the downward branch of the direct circulation and shifts it toward the warm side of a developing upper-level front. Thus, a direct secondary circulation can have the appearance of being locally indirect. Later observations by Cammas and Ramond (1989) support this finding. Aside from resolving the direct/indirect circulation contradiction, only with the addition of cold advection to geostrophic confluence does the two-dimensional model produce frontal zones sufficiently deep to match the observed cases mentioned above (Keyser and Pecnick 1985; Reeder and Keyser 1988).

The question has been raised whether two-dimen-

sional models, such as that used by Keyser and Pecnick (1985) and Reeder and Keyser (1988), can adequately represent upper-level fronts. Newton and Trevisan (1984), based on their three-dimensional simulations, asserted that the combination of cross-stream and along-stream circulations (the latter being related to curvature effects) gives a more complete picture of frontogenesis than either individual component. Keyser et al. (1989), however, found both the pattern and magnitude of the vertical motion to be dominated by the cross-front component of the divergent wind, with the alongfront component having a subordinate effect on the frontogenesis. Keyser and Shapiro (1986, p. 489) point out that the pattern of the transverse flow in Newton and Trevisan (1984) upstream of the trough base closely resembles the pattern from the cold advection case of Keyser and Pecnick (1985). Similarly, Keyser et al. (1989, 1992) demonstrate in a three-dimensional model simulation similar to that of Newton and Trevisan (1984) that frontogenesis and tropopause folding forced by cold advection and confluence occurs downstream of the inflection point between a trough and its upstream ridge. Bosart (1970), in an observational study, identified changes in frontogenetical forcing through the evolution of an amplifying baroclinic wave. These results, and conclusions by Hines and Mechoso (1991), suggest that although a two-dimensional treatment of upper-level frontogenesis and tropopause folding can be accurate locally, such findings cannot be generalized for the entire baroclinic wave structure and life cycle, where different forcing mechanisms may be present.

The preceding review highlights the importance of considering the synoptic regime in which upper-level phenomena are developing. The divergence and vertical motion patterns associated with upper-level fronts are intricately related to midlatitude cyclogenesis, but the direction of causality has yet to be determined (Keyser and Shapiro 1986).

b. Review of RSS

RSS is a recent example of a traditional, three-dimensional numerical study of upper-level frontogenesis within a developing baroclinic wave. Using a methodology designed by Hoskins (1982), RSS diagnose the frontogenetical forcing by the geostrophic wind in terms of the **Q** vector. They infer the three-dimensional ageostrophic wind field from the pattern of **Q** and determine whether it reinforces or counteracts the frontogenetical effect of the geostrophic wind. Finally, they examine whether air parcels reside in regions where the geostrophic and ageostrophic forcing act in concert (a positive feedback) long enough for a front to form.

This methodology is applied to data derived from an f-plane primitive-equation channel model formulated in height coordinates that is dry, adiabatic, hydrostatic, Boussinesq, and inviscid except for a fourth-order horizontal diffusion term. The domain of integration is $x \in (0, x_L = 4000)$ km, $y \in (0, y_L = 8000)$ km, and $z \in (0, H = 15)$ km. The grid spacing is 100 km in the horizontal and 0.25 km in the vertical. The flow is periodic in the x direction and there is no flow normal to the meridional or horizontal boundaries. The Coriolis parameter $f_0 = 10^{-4}$ s^{-1} and density $\rho_0 = 1$ kg m^{-3}. The basic state has a constant PV ($\sim$0.4 PVU; 1 PVU $= 10^{-6}$ m^2 s^{-1} K kg^{-1}) troposphere smoothly joined to a constant PV ($\sim$3.6 PVU) stratosphere. An upper-level jet stream, associated with a locally steep tropopause, flows from west to east through the center of the domain (RSS, their Fig. 11). The model is initialized with a small but growing perturbation with a doubling time of roughly 1 day and a phase speed of 23 m s^{-1}.

Figure 1 shows the evolution of the upper wave and distribution of **Q**, while the frontogenesis function [RSS, their Eqs. (6)–(9)] is plotted for days 7 and 9 in Figs. 2 and 3, respectively. Early on (days 6 and 7), the horizontal frontogenesis is dominated by the geostrophic wind, with weak confluence south of and diffluence north of the northwesterly jet from ridge to trough (Figs. 1a,b). The geostrophic forcing is frontogenetical where **Q** points toward warmer air (Figs. 1b and 2a). This pattern induces an ageostrophic response with horizontal flow toward the jet (the upper-level ageostrophic winds are approximately antiparallel to **Q**) and sinking along it, such that tilting dominates the overall frontogenesis from the northwesterly flow inflection point to the base of the trough (Figs. 2c,d). The subsidence brings down higher-θ air, leading to a configuration of cold advection and confluence (cf. days 6 and 7 in Figs. 1a,b). This configuration further strengthens the vertical motion field and increases the divergence of **Q** in the manner of Shapiro (1981) and Keyser and Pecnick (1985). This positive feedback, whereby tilting increases the divergence of **Q**, leading to increased vertical motions, which produce stronger tilting, is responsible for the frontal intensification near the trough base and continues until the upper-level thermal gradient weakens in the low (day 9, Fig. 1d), curbing the geostrophic forcing in the low and leading to primarily alongfront ageostrophic flow near the low. Tilting still forces frontogenesis, but the feedback mechanism has now shut down. RSS conclude that, at this time (day 9, Fig. 3), the horizontal terms dominate in the region upstream of the northwesterly flow inflection point, with both geostrophic and ageostrophic frontogenesis contributing significantly, while farther downstream they cancel each other, allowing tilting to dominate.

RSS give a comprehensive, self-consistent description of upper-level frontogenesis that builds on previous theoretical and observational studies. However, their diagnosis requires the Lagrangian computation of various terms in the frontogenesis equation following selected air parcels within the frontal zone, making a synoptic view of the processes responsible for frontal development difficult. The division of frontogenesis into terms involving the geostrophic, ageostrophic, and vertical

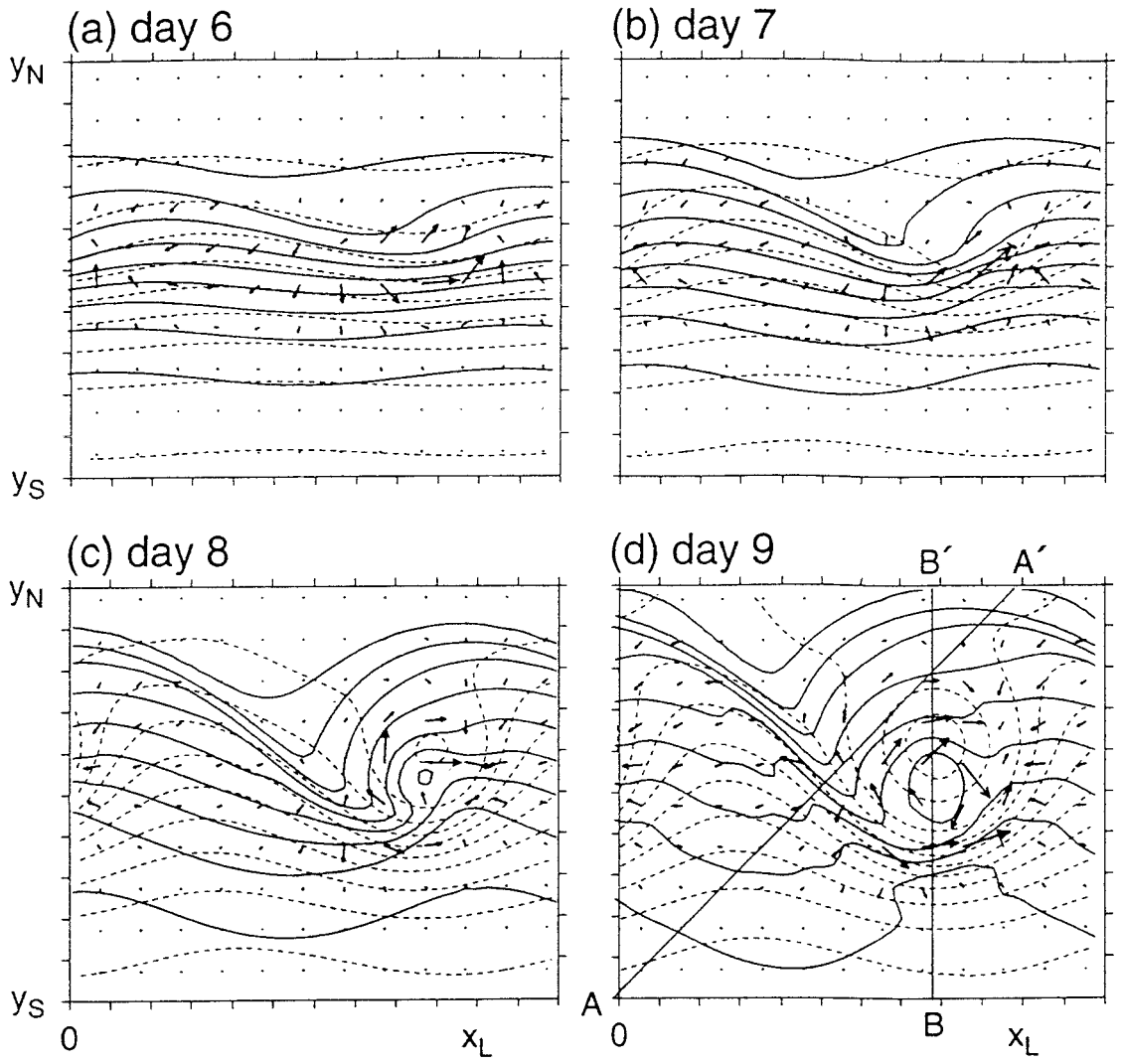

FIG. 1. Evolution of potential temperature θ [solid lines, contour interval (CI) = 5 K], geopotential ϕ (dashed lines, CI = 1000 m^2 s^{-2}), and **Q** (vectors plotted every $4\Delta x$; units not relevant) at $z = 6$ km for $x \in (0, 4800)$ km (wave relative) and $y \in (2000, 6000)$ km for (a) day 6, (b) day 7, (c) day 8, and (d) day 9. From RSS (Fig. 13).

wind components is not unique; an alternative partitioning into nondivergent and irrotational components of the three-dimensional wind may be preferable in areas of strongly curved flow where the transverse circulation (v_{ag}, w) fails to satisfy mass continuity (Keyser et al. 1989). For an extensive treatment of the issues concerning the representation of frontal circulations, the reader is referred to Keyser (1999).

A final possible shortcoming to the conventional description of upper-level frontogenesis may be the focus on frontogenesis itself. The classical description of cyclogenesis in terms of vertical motion forced by vorticity and temperature advection has been supplemented in recent years by the PV viewpoint (e.g., Hoskins et al. 1985; Davis and Emanuel 1991). The PV viewpoint emphasizes the dynamically crucial role of PV gradients, and development takes place primarily through the quasi-horizontal advection of PV by the balanced wind. The dimensionality of the problem is effectively reduced by one under the constraint of adiabatic flow: vertical motions, instead of being central, are secondary and required only to maintain thermal wind balance as the PV distribution evolves, and the crucial PV advections take place on two quasi-horizontal surfaces: the ground and the deformable tropopause. In this paper, we suggest that focusing on PV redistribution is as advantageous for understanding upper-level frontogenesis as it is for understanding cyclogenesis.

3. Data and methodology

a. Definition of the tropopause

The tropopause often is defined as a surface of constant PV (Hoerling et al. 1991; Morgan and Nielsen-

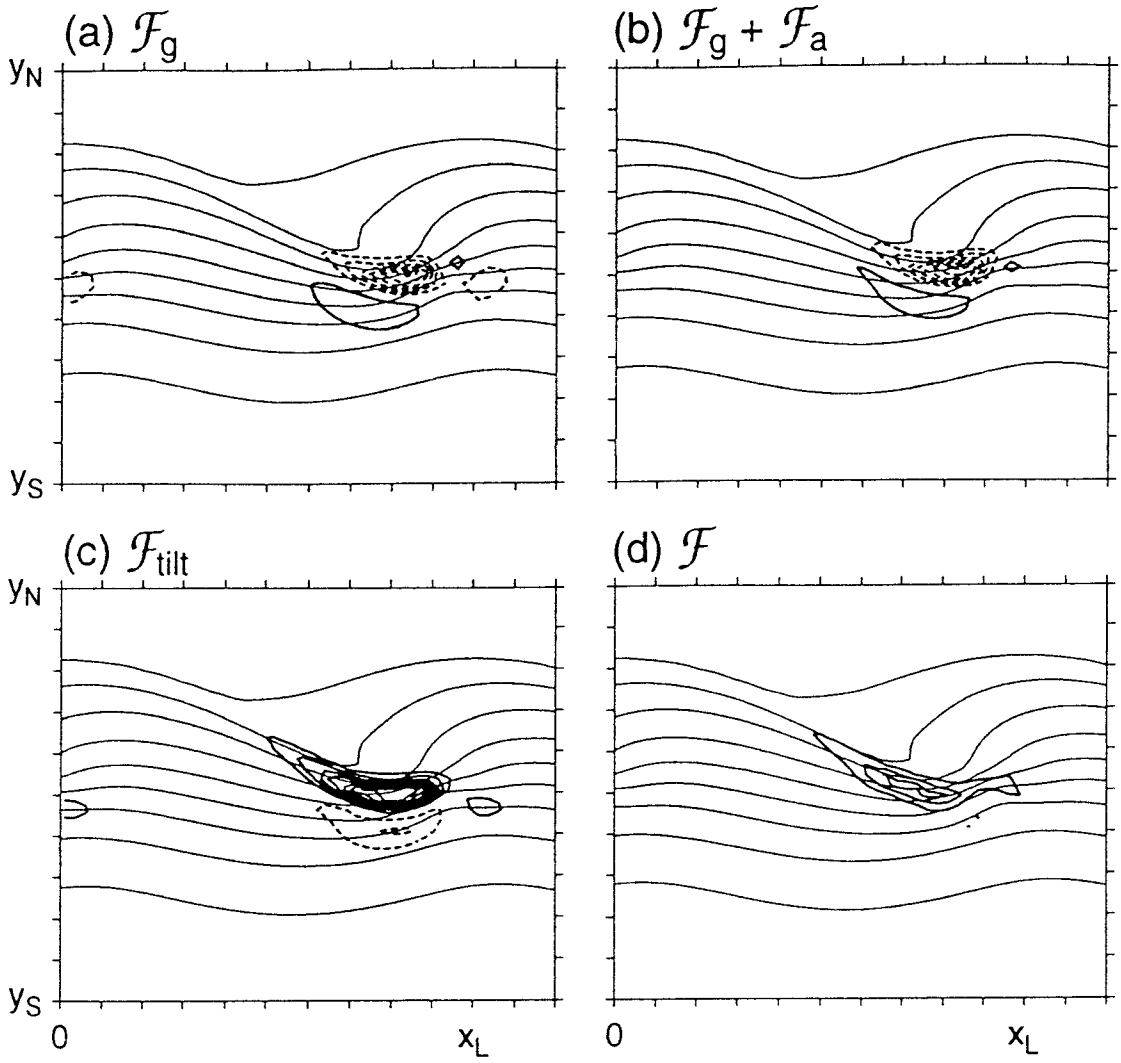

FIG. 2. Plot of θ (light solid lines, CI = 5 K) at day 7 at z = 6 km on the same domain as shown in Fig. 1c displayed with (a) F_g, (b) $F_g + F_a$, (c) F_{tilt}, and (d) F. For all F, CI = 20 [K (100 km)$^{-1}$]^2/10^5 s. From RSS (Fig. 19).

Gammon 1998). Such a tropopause is known as a dynamic tropopause. In the absence of diabatic and frictional processes, the dynamic tropopause is a material surface, and even when PV is not conserved the dynamic tropopause tends to exhibit better spatial and temporal continuity than a tropopause defined in terms of lapse rate.

In the RSS baroclinic life cycle model, the tropopause is analytically specified to coincide with a jump in PV from ~0.4 to ~3.6 PVU. In principle, therefore, any value of PV within that range could be used to define the tropopause. However, because the model contains a finite grid spacing, the tropopause is not truly discontinuous. Furthermore, because of explicit and numerical diffusion, PV is not strictly conserved, and the fraction of fluid volume intermediate between tropospheric and stratospheric PV values gradually increases with time.

To determine an appropriate definition of the tropopause, the model was initialized with a passive tracer with uniform and distinct values in the troposphere and stratosphere. This passive tracer was advected conservatively during the simulation, and the location of the passive tracer surface midway between tropospheric and stratospheric values was compared to the location of various PV surfaces. The 1.8-PVU surface corresponded most closely to the passive tracer surface; therefore, the tropopause is defined as the 1.8-PVU surface in this paper. Where the 1.8-PVU surface is found multiple times in a given grid column, the highest occurrence of this surface is defined as the tropopause.

b. Tools for analyzing tropopause folding

RSS focused on the rate of change of the horizontal potential temperature gradient as forced by geostrophic, ageostrophic, and vertical components of the wind field.

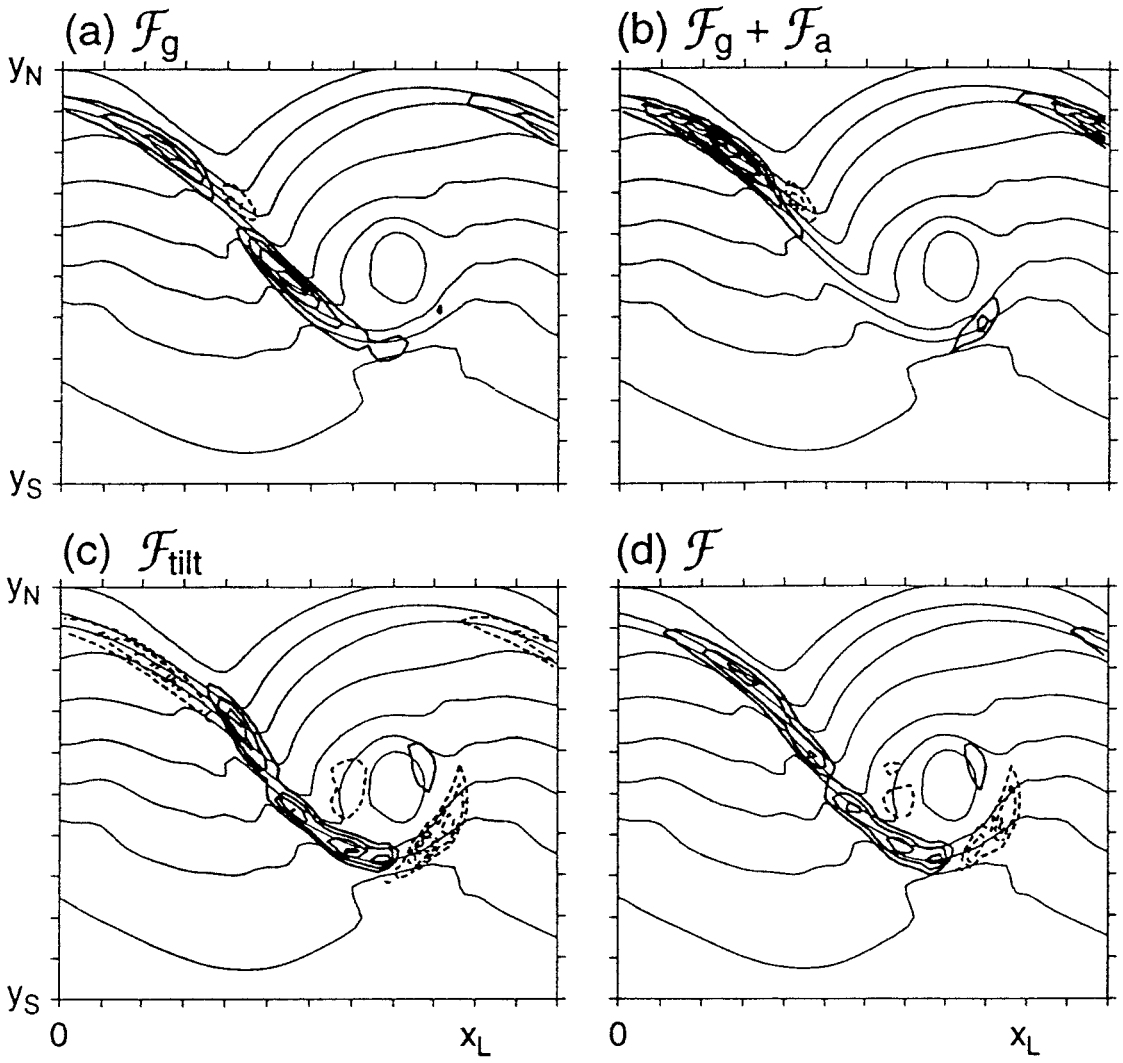

FIG. 3. As in Fig. 2, but for day 9. From RSS (Fig. 20).

As mentioned previously, when viewed from a PV framework the focus shifts from frontogenesis to tropopause folding, or foldogenesis. While developing a kinematic description of foldogenesis, we will no longer concentrate on the idea of geostrophic forcing and ageostrophic response.

On an f plane, three-dimensional circulations are defined by the irrotational and vertical velocities. Keyser et al. (1992) argue that this three-dimensional circulation is ''the natural extension of the transverse secondary circulation that arises in two-dimensional frontogenesis theory.'' The following discussion of how to obtain the partitioned winds is taken from Keyser et al. (1989, 1992), to which the reader is referred for a complete treatment of the subject.

To obtain the irrotational wind field in a channel model, it is first necessary to find the velocity potential by inverting

$$\nabla_z^2 \chi = -\frac{\partial w}{\partial z}, \tag{1}$$

where χ is periodic in x. For the meridional boundaries,

$$\chi(y = 0) = 0, \qquad \chi(y = y_L) = y_L \overline{v}_{ag}, \tag{2}$$

where the overbar represents a domain-areal average at a given level. From (1) and (2), the irrotational wind field may be determined:

$$\mathbf{v}_{ir} = \boldsymbol{\nabla}_z \chi. \tag{3}$$

The basic-state wind, $\mathbf{v}_b$ $[=u_b(y, z)\hat{\mathbf{i}}]$, is entirely nondivergent; see the appendix of RSS for a complete specification. The remaining nondivergent wind, $\mathbf{v}_{nd}$, which grows during the simulation, can then be obtained from the definition $\mathbf{v}_{nd} = \mathbf{v} - \mathbf{v}_{ir} - \mathbf{v}_b$. The total three-dimensional motion field thus consists of $\mathbf{v}_b$, $\mathbf{v}_{nd}$, and $(\mathbf{v}_{ir}, w)$.

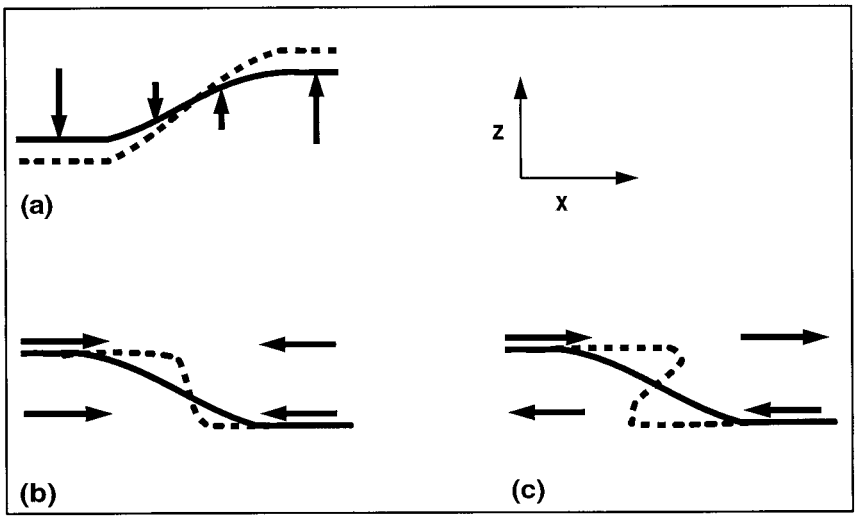

FIG. 4. Schematic diagrams of foldogenesis. The thick solid and dashed lines denote the tropopause at times t_0 and $t_0 + \Delta t$, respectively. Arrows indicate sense and magnitude of the winds in the vicinity of the tropopause. (a) Diagram illustrating differential vertical motion. If the gradient of the vertical motion is of the same sense as the height gradient, the tropopause steepens. (b) Diagram illustrating confluence/convergence. The differential advection of the tropopause causes it to steepen, but as the tropopause approaches vertical the differential advection decreases. (c) Diagram illustrating vertical shear. The winds along the tropopause are identical to the confluence/convergence case at t_0, but differential advection by the vertical shear continues after the tropopause becomes vertical to produce a tropopause fold.

Just as the RSS frontogenesis function measures the effect of various wind components on the horizontal potential temperature gradient, our foldogenesis function quantifies the effect of the wind on the slope of the tropopause. This function has the form

$$F = \frac{d|\nabla z_T|}{dt} = F_h + F_w, \tag{4}$$

$$F_h = \hat{\mathbf{n}} \cdot \left[-\left(\frac{\partial u}{\partial x}\frac{\partial z_T}{\partial x} + \frac{\partial v}{\partial x}\frac{\partial z_T}{\partial y} \right)\hat{\mathbf{i}} - \left(\frac{\partial u}{\partial y}\frac{\partial z_T}{\partial x} + \frac{\partial v}{\partial y}\frac{\partial z_T}{\partial y} \right)\hat{\mathbf{j}} \right], \tag{5}$$

$$F_w = \nabla w \cdot \hat{\mathbf{n}}, \tag{6}$$

where z_T is the height of the tropopause, all wind components are interpolated to the tropopause surface, the gradient operator is evaluated along the tropopause surface, and $\hat{\mathbf{n}}$ $(=\nabla z_T/|\nabla z_T|)$ is a horizontal unit vector oriented in the direction of the gradient of tropopause height. Equation (4) is the standard form of Petterssen's frontogenesis equation (Petterssen 1956, p. 202; Bluestein 1993, p. 253) with z_T substituted for θ. Substitution of the basic-state, nondivergent, and irrotational winds, interpolated to the tropopause, into the horizontal term F_h yields F_b, $F_{\rm nd}$, and $F_{\rm ir}$, respectively, where $F_h = F_b + F_{\rm nd} + F_{\rm ir}$.

A schematic diagram of the various terms of the foldogenesis equation is shown in Fig. 4. The solid line denotes the tropopause viewed in cross section at $t = t_0$ and the dashed line at $t = t_0 + \Delta t$. The arrows represent the winds at the tropopause level. Contributions by the vertical term are due to differential vertical motion and not merely to lifting or sinking. The latter only will displace the tropopause surface upward or downward, while the former causes a change in the slope of that surface. Tropopause steepening occurs where the horizontal gradient of the vertical motion has a component parallel to the tropopause height gradient, as in Fig. 4a, regardless of whether that vertical motion is upward or downward. An antiparallel alignment of the vertical motion and height gradients leads to a flattening of the tropopause.

Proper alignment of the height gradient and the horizontal winds can also lead to a steepening of the tropopause. Both horizontal confluence/convergence (Fig. 4b) and vertical shear (Fig. 4c) can induce a change of tropopause slope, but only vertical shear can produce a folded tropopause. In the absence of vertical shear, the tropopause can approach vertical but cannot fold. Note that if the tropopause is initially flat, purely horizontal motions cannot generate a slope ($F_h = F_{\rm ir} = F_{\rm nd} = F_b = 0$). Conversely, vertical motions have little effect on the slope of an already steep tropopause, which can only become folded by horizontal motions.

As the tropopause folds, the quantitative foldogenesis diagnosis itself ultimately breaks down for the following reasons.

1) As the tropopause surface becomes vertical, the slope approaches infinity, and it is no longer appropriate to diagnose changes in slope.

2) As the tropopause folds, the tropopause surface becomes multiply valued.

Diagnosing changes in intensity of a tropopause fold would require a definition of the intensity or strength of a tropopause fold. One possible measure is the horizontal distance that the stratospheric air extends into the tropospheric air. This might be called the width of the fold. A kinematic diagnosis of fold intensity would involve determining the rate of change of the width of the fold in some Lagrangian sense, perhaps by measuring the flux of stratospheric air into or out of the fold.

Even before the diagnosis of a developing fold becomes mathematically or physically inappropriate, the finite-difference computation of foldogenesis becomes inaccurate. A vertical or nearly vertical tropopause cannot be resolved on a conventional grid and will be aliased as a steep slope spanning the distance between adjacent grid points. Since the tropopause slope itself is underestimated, the horizontal foldogenesis terms will be underestimated relative to the vertical term.

Fortunately, useful information still is available from the diagnosis of horizontal foldogenesis in the model even when the true tropopause is folded. Even on days 7 and 8, where the true tropopause becomes vertical or folded and foldogenesis loses its original interpretation, positive values of the horizontal terms of the foldogenesis equation imply a strengthening of the tropopause fold in the sense of positive mass flux into the folded region of the stratosphere, and the relative importance of the various horizontal terms to this process still can be diagnosed.

c. Piecewise quasigeostrophic potential vorticity inversion

In order to assess the role of surface cyclogenesis in tropopause folding, it is necessary to distinguish the extent to which the upper-level winds are attributable to lower-level features. It is for this reason that PV diagnostics are employed here.

Potential vorticity has become an increasingly useful tool in synoptic meteorology, thanks to the seminal paper by Hoskins et al. (1985) that laid the groundwork for PV diagnostic techniques. Given the spatial distribution of PV, one can calculate the geopotential height field and the entire balanced three-dimensional wind field (Davis et al. 1996). This inversion requires 1) specification of a balance condition (e.g., geostrophic), 2) specification of an approximate form of PV consistent with the balance condition, 3) definition of some form of a reference state (e.g., zonal mean), and 4) solution of the problem globally, with proper boundary conditions. The fourth requirement results from the fact that the geopotential height and wind at a given point, (x_0, y_0, z_0), are determined by the distribution of PV throughout the entire domain, not simply by PV (x_0, y_0, z_0), and so the PV must be inverted over the entire domain to determine the geopotential height and wind at (x_0, y_0, z_0).

Hoskins et al. (1985) illustrate PV diagnostics utilizing Ertel PV and a gradient wind balance system. This approach can render calculations quite cumbersome. The same holds for the nonlinear balance system employed by Davis and Emanuel (1991), Davis (1992), and Davis et al. (1996). To avoid these complications, Nielsen-Gammon and Lefevre (1996) and Hakim et al. (1996) turned to quasigeostrophic potential vorticity (QGPV), where on an f plane,

$$\text{QGPV} = q = \frac{1}{f_0}\nabla_z^2\phi' + f_0 + f_0\frac{\partial}{\partial z}\left(\frac{1}{N^2}\frac{\partial\phi'}{\partial z}\right). \quad (7)$$

In (7), ϕ' is defined as the departure from the basic-state ϕ, where ϕ is the pressure variable. In a Boussinesq, height-coordinate model, geopotential and pressure differ only by a constant of proportionality, and to be consistent with standard terminology deriving from the use of isobaric coordinates we will refer to pressure fields hereafter as geopotential (or geopotential height) fields. In addition to computational simplicity, a major advantage of the QG system is the linearity of QGPV and thus of the QGPV inversion (Davis 1992).

Linearity is particularly advantageous for the piecewise inversion technique in which the influence of one part of the PV field is isolated by setting the rest of the field to zero. In this way, solving (7) for ϕ' will recover a partial geopotential from which the flow attributed solely to the isolated PV feature can be calculated. In contrast, nonlinear balance requires an arbitrary linearization in order to perform piecewise inversions (Davis and Emanuel 1991). Nielsen-Gammon and Lefevre (1996) partitioned QGPV into upper and lower layers to assess the extent to which a lower-level anomaly can influence the development of an upper-level mobile trough. The same partitioning and inversion technique will be used here. Juckes (1999) shows that the QGPV inversion approach is valid at small Rossby number even in the presence of a strongly sloped tropopause with a PV discontinuity.

To the greatest extent possible, the upper layer must include the PV variations associated with the tropopause and the lower layer must exclude them. With QGPV, this division cannot be accomplished perfectly because an intense vortex embedded in a uniform PV environment will feature associated QGPV anomalies that extend vertically beyond the level of the Ertel PV anomaly (Davis 1992). Furthermore, in the RSS model simulations, Ertel PV is generated at the lower boundary and ultimately extends upward to a height of several kilometers, with a corresponding impact on the QGPV field. The optimal division between upper and lower QGPV is found at 3125 m, and this dividing level is used in all piecewise PV inversions. It should be borne in mind that, by day 8, a clean separation between upper-layer

and lower-layer PV can no longer be made, although we still expect qualitative interpretations to be possible.

To obtain the perturbation geopotential height field associated with a given layer of QGPV, the QGPV in the other layer and the perturbation potential temperature along the exterior horizontal boundary of that layer (i.e., the ground or lid, as appropriate) are set to zero, and the remaining QGPV is inverted with (7), using the remaining inhomogeneous boundary condition on perturbation potential temperature. Once these perturbation geopotential height fields are found, the wind fields associated with each anomaly can be calculated and their role in foldogenesis determined.

There are limits to what partitioning can yield. For example, it was previously shown that the irrotational component of the total horizontal wind field can be obtained from the vertical motion field. Partitioning the irrotational flow into upper and lower components would first require separating the vertical motion field into upper and lower layers, as is done with the PV field. While this can be done mathematically, there is no physically meaningful justification for such a partitioning of w. Similarly, there is no meaningful layer partitioning of the ageostrophic vorticity, from which the upper and lower components of $\mathbf{v}_{agnd}$ would be obtained [Keyser et al. (1989); their Eqs. (3.7)–(3.10)]. The absence of the ageostrophic component of the nondivergent wind leads to an overestimate of the contribution of the nondivergent component of the foldogenesis function in the trough and an underestimate in the ridge. This error, which is very small at day 5, increases with time as the flow curvature increases but does not introduce qualitative errors into the diagnosis even at day 7. Recently, a method has been proposed to partition the irrotational flow into upper and lower components (Morgan 1999); such a diagnosis is beyond the scope of this paper and will be explored in a future article. Therefore, the partitioned wind fields are restricted to their geostrophic components, since these may be diagnosed directly from the partitioned perturbation geopotential height fields obtained from (7).

d. Tropopause maps

Before getting into the details of the tropopause folding, it is beneficial to examine the evolution of the baroclinic wave in the RSS model. Figure 5 shows the surface cyclone evolution from day 5 through day 8. The surface warm and cold fronts form between days 6 (Fig. 5b) and 7 (Fig. 5c). By day 8 (Fig. 5d), the system is fully occluded and the rate of intensification has slowed (note the changing contour interval for the perturbation geopotential field). The upper-level wave develops more slowly (Fig. 1), with a front beginning to form on day 7 (Fig. 1b) in the base of the trough. Day 8 (Fig. 1c) shows the upper-level front extending back upstream toward the ridge. Meanwhile, in the base of the trough, the upper-level front has descended to near 4 km between days 7 and 8 (Fig. 6; see also Fig. 7). RSS show that the tropopause has become folded along a considerable length of the upper-level front at these times.

To investigate the structure and evolution of the tropopause fold, we shift from constant-height maps to a constant-PV map, specifically a tropopause map. Figure 7a shows a sample tropopause map from day 8 with contours of tropopause height. The dotted and small-dashed contours depict a high tropopause, while the thick solid and long-dashed contours depict a low tropopause. This and the following tropopause maps were constructed using the contour superposition method (Morgan and Nielsen-Gammon 1998), which permits depiction of a folded tropopause. In Fig. 7a, the tight packing of the dotted and small-dashed contours along the track of cross section AB indicates a steeply sloped tropopause, and the superposition of the small-dashed and thin solid contours signifies a vertical tropopause. Near the base of the trough, the thick solid, closed contour (4375 m) extending southward beyond all the others shows a tropopause fold. The cross section (Fig. 7b) provides a side view of the tropopause surface and illustrates that tropopause folding and upper-level frontogenesis are coincident phenomena. It should be noted that although the upper-level front is relatively weak, the portion of the fold sampled in Fig. 7b has evolved from a nearly flat tropopause.

Figure 8 shows the evolution of the tropopause. At day 5 (Fig. 8a) the tropopause is nearly undisturbed from its initial configuration of a steep slope along a 70 m s^{-1} westerly jet. The thin solid contour on day 5 (Fig. 8a) shows where an initially flat region of the tropopause has begun to sink. By day 7 (Fig. 8c), the tropopause is nearly vertical near the base of the trough. Comparison with Fig. 6a (on which the 6125-m tropopause contour has been added) shows this to be the location of the nascent upper-level front in Fig. 1b. Likewise, the extension of the nearly vertical region of the tropopause upstream toward the ridge on day 8 (Fig. 8d) coincides with the evolution of the upper-level front in Figs. 1c, 6b, and 7. At the same time, the higher contours of tropopause height have attained a wavelike structure. This ''tropopause height wave'' corresponds to a wave in the PV field on those height surfaces that intersect the tropopause, and henceforth it will be referred to as a PV wave.

4. Results

Tropopause maps and the foldogenesis function now will be employed to answer some issues unresolved in RSS, such as determining the processes responsible for producing the nascent upper-level front that RSS studied on day 7, and those responsible for dictating the location of the tropopause fold within the baroclinic wave. Consequently, the analyses presented below begin with day 5, before the front is evident. By day 8, the surface

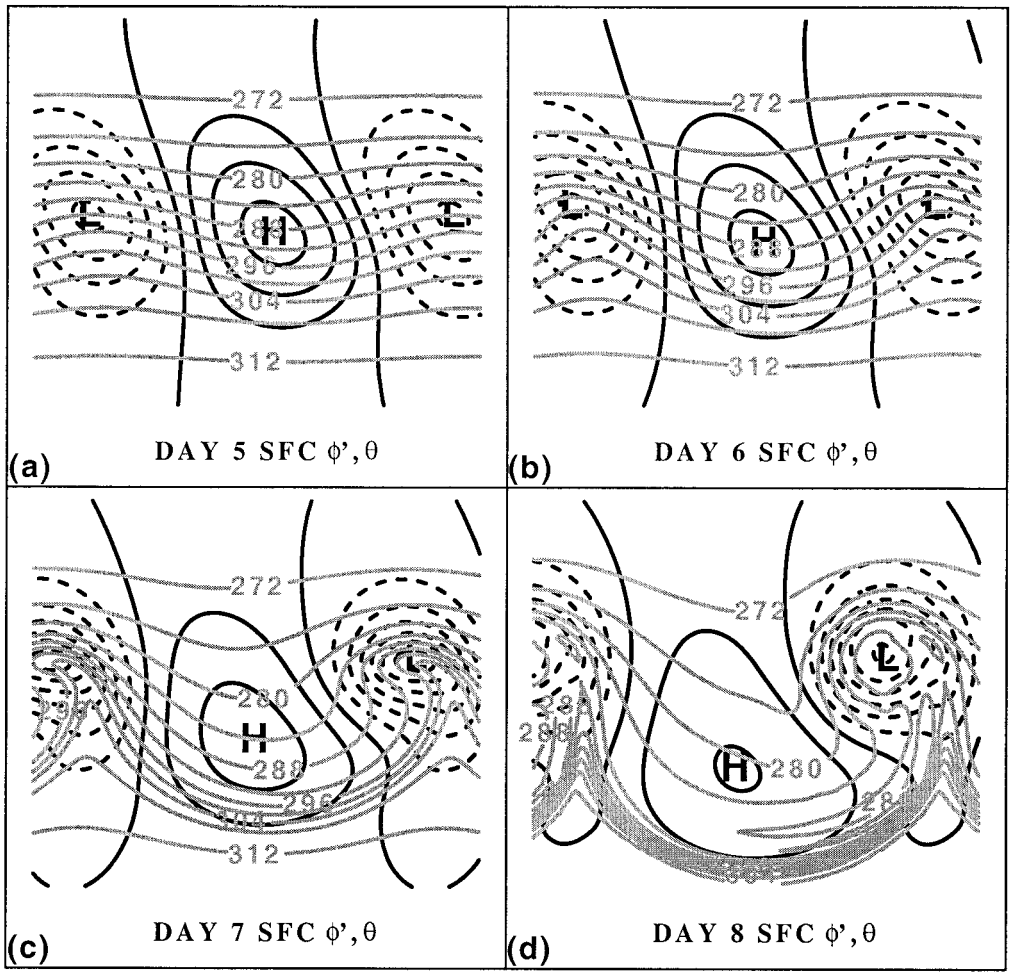

FIG. 5. Time sequence of θ (gray contours, CI = 4 K) and ϕ' (black contours, negative dashed) at the surface for $x \in (0, 5000)$ km (wave relative) and $y \in (1800, 6000)$ km at (a) day 5, CI = 100 m^2 s^{-2}; (b) day 6, CI = 200 m^2 s^{-2}; (c) day 7, CI = 500 m^2 s^{-2}; (d) day 8, CI = 1000 m^2 s^{-2}. ϕ' extrema are denoted by an L for minima and H for maxima.

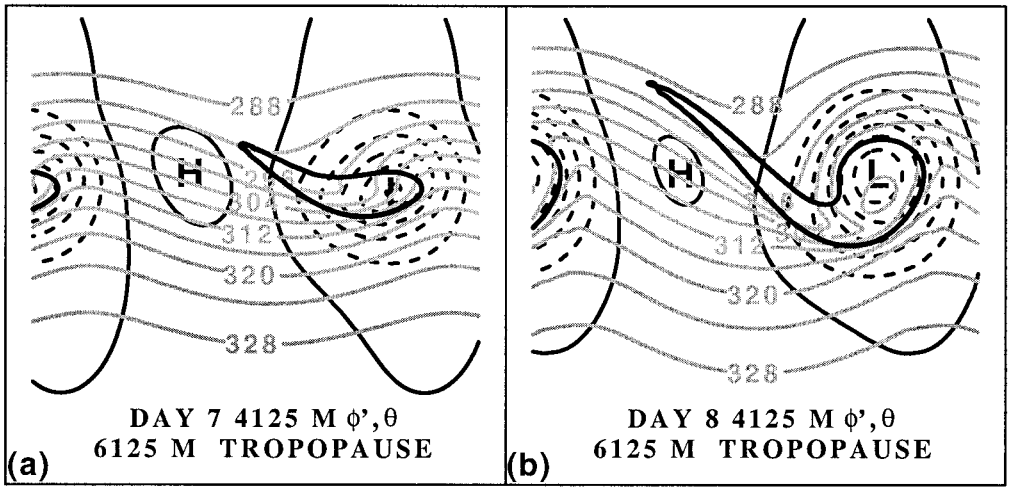

FIG. 6. As in Fig. 5, except at 4125 m. Contour intervals for θ are 4 K, and at (a) day 7, ϕ' CI = 400 m^2 s^{-2}; (b) day 8, ϕ' CI = 800 m^2 s^{-2}. Also plotted is the tropopause (1.8-PVU contour) at 6125 m.

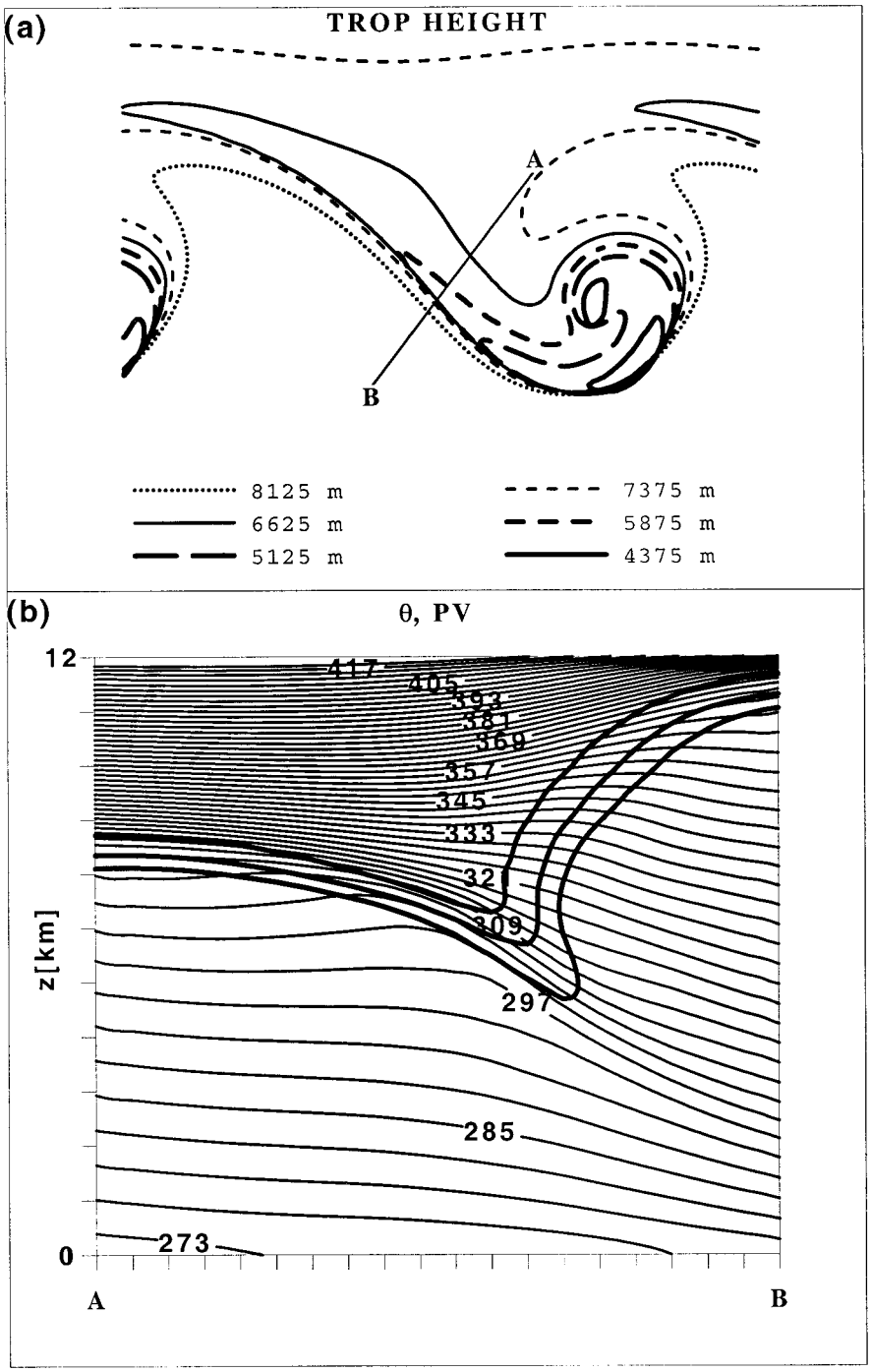

FIG. 7. (a) Tropopause height z_T at day 8 (contour values at and below 8125 m are indicated in the figure), and (b) vertical cross section at day 8 showing θ (light contours, CI = 3 K) and PV (heavy contours marking the 1.0-, 1.8-, and 3.0-PVU surfaces) for a NE–SW section through the northwesterly flow, shown in (a). Domain in (a) is the same as in Fig. 5 except $y \in$ (2500, 6500) km.

cyclone is occluded (Fig. 5d) and the upper low has cut off (Fig. 1c)—wave development has nearly ceased. No results are presented beyond day 8 because of the unrealistic cyclone and frontal structures that ultimately evolve once the growing normal mode has attained large amplitude in the periodic channel.

Figure 9 shows the evolution of foldogenesis from day 5 through day 8. Of particular interest is the con-

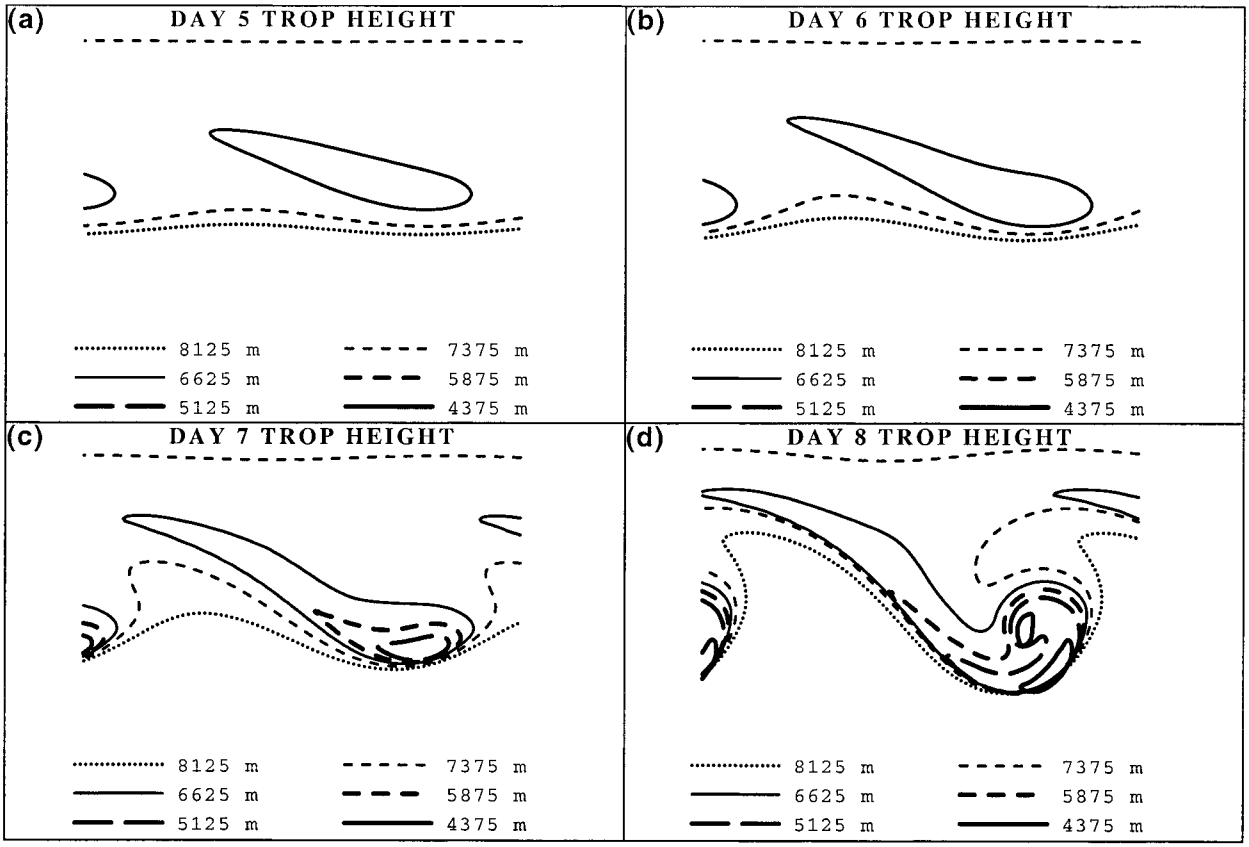

FIG. 8. Time sequence of tropopause height z_T on the same domain as in Fig. 7a: (a)–(d) are the same times as in Fig. 5. Contour values at and below 8125 m are indicated in the panels.

sistency throughout the period. The foldogenesis function strengthens by nearly two orders of magnitude between days 5 and 8, and the regions of foldogenesis and foldolysis constrict along the tropopause height gradient, but the basic pattern, including foldogenesis upstream of the trough and foldolysis downstream, remain throughout the evolution of the baroclinic wave. In other words, the processes that lead to the fold already are fully active during the quasi-linear growth stage of the baroclinic wave, three days prior to the appearance of the fold.

a. Day 5

Figure 10 shows the separate contributions by the individual components of the foldogenesis function at day 5. The horizontal terms (Figs. 10a–c) are primarily focused along the initial tropopause slope (though the stronger basic-state wind is starting to act on the newly sloped region), while the vertical term (Fig. 10d) is generating a slope in the initially flat area of the tropopause north of the slope and upstream of the trough axis.

Vertical motion acts to increase the slope in some areas and decrease it in others, which can be seen by looking at the vertical motion field itself. The shading in Fig. 11a represents the vertical motion field at the tropopause. The maximum lifting is beneath the initially low tropopause upstream of the upper-level ridge. The lower (northern) region of the tropopause is lifted more than the higher (southern) region, leading to a flattening of the initial gradient in this area (cf. Fig. 10d). Conversely, northeast of the upward motion maximum, where the tropopause is initially flat, the same differential lifting works to create a slope. The downward motion produces an analogous dipole upstream of the upper-level trough (Fig. 10d). Also shown in Fig. 11a is the irrotational wind field, which diverges from the upward motion maximum. The confluence/convergence along the initial tropopause height gradient in the base of the trough and the diffluence/divergence along this gradient in the ridge help to increase the slope in the trough and to flatten the slope in the ridge (Fig. 10a).

Figure 11b displays the nondivergent flow at the tropopause, as defined in section 3b. The clockwise and counterclockwise rotations correspond to the locations of the upper-level ridge and trough, respectively. Between these, east of the ridge, the predominantly northerly winds along the lower region of the tropopause (north of the slope) are stronger than those along the higher region (south of the slope), increasing the initial

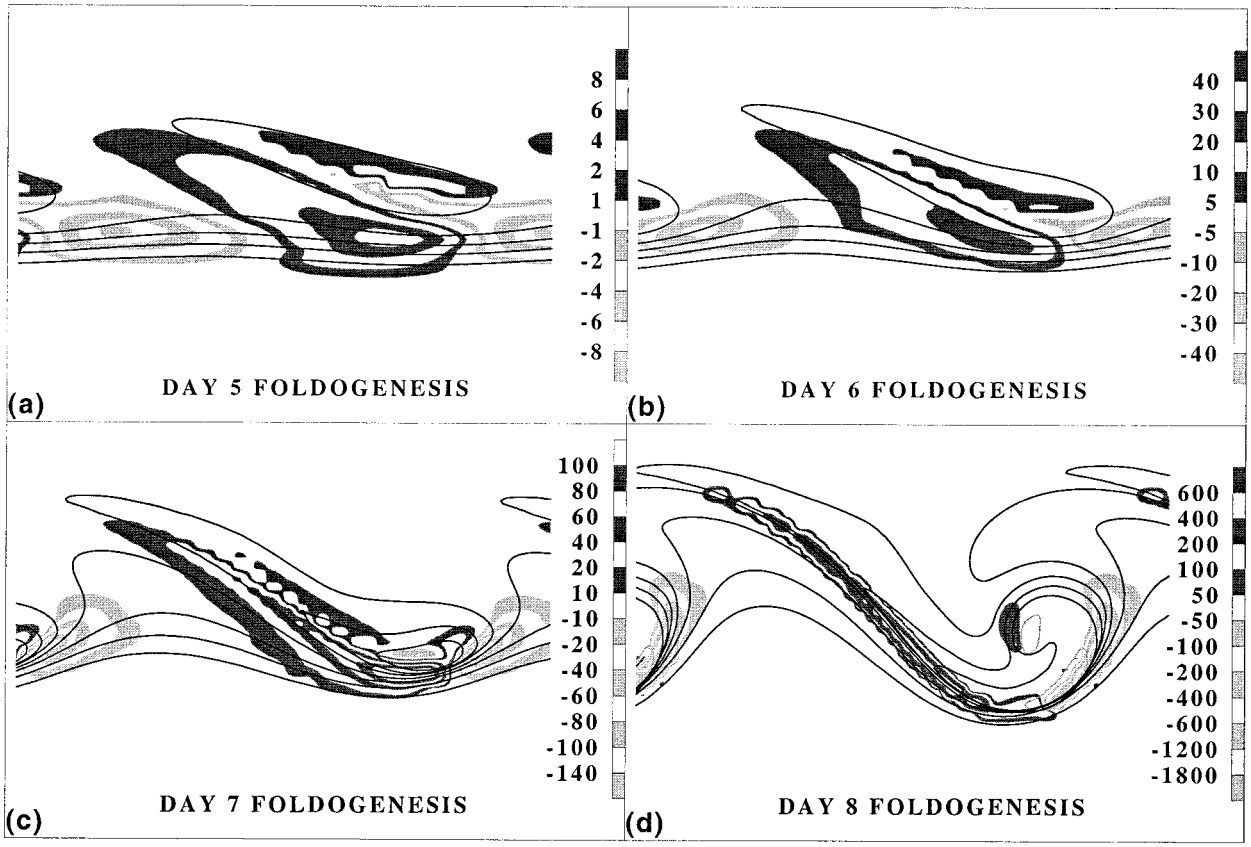

FIG. 9. Tropopause height z_T as in Fig. 8 (with the addition of the 8875- and 9625-m contours) but including the foldogenesis function [10^{-8} s^{-1}, shaded]. Shading intervals are indicated in the panels. Domain is the same as in Fig. 8, except $y \in$ (3000, 6000) km.

gradient (Fig. 10b). West of the ridge, the predominantly southerly winds along the lower region of the tropopause are again stronger than those along the higher region, thus acting to flatten the slope. The basic-state wind (Fig. 11c) is roughly parallel to the initial slope, but it does have a small cross-tropopause component. (The zonal phase speed of the linear wave, 23 m s^{-1}, which is representative of the speed of the simulated wave throughout the period of interest, has been subtracted from the basic-state wind vectors for clarity; note that changing the wind field by a uniform additive factor does not affect its foldogenetical properties.) The alongstream variation of basic-state wind speed is a manifestation of its vertical shear and the varying height of the tropopause. In this context, the vertical shear acts to increase the tropopause slope upstream of the trough (as shown schematically in Fig. 4c) and to decrease it downstream of the trough (Fig. 10c) along the lower region of the tropopause (north of the slope). [This action by the basic-state wind will be more evident in the higher-amplitude wave at day 7 (Fig. 12c).]

Streamlines of the wave-relative total wind field are shown in Fig. 11d. The elongated shape of the depressed tropopause is not related directly to the vertical motion pattern, which deviates little from a simple two-cell pattern, but instead may be explained kinematically in terms of the confluent streamline and motion of air parcels relative to the wave, as follows: The cyclonic shear north of the jet rotates the axis of maximum vertical displacement into a northwest–southeast orientation, aligning it with the confluent streamline that extends from the saddle point near the ridge to the closed circulation north of the trough. Near the inflection point along the confluent streamline between the trough and upstream ridge, sinking is weak, but the wave-relative horizontal flow northeast of the confluent streamline is very weak, signifying that air parcels have a long residence time in the region of sinking. Southwest of the confluent streamline, air parcels have recently come through the lifting maximum with a relatively short history of weak sinking. In effect, there is differential vertical displacement, which is responsible for the existence and orientation of the depressed region of the tropopause. The tilting by this differential vertical motion at day 5 produces the significant slope of the tropopause seen two days later (Fig. 8c). The slope in the northwesterly flow region at day 7, although significant, could hardly be called steep, but it is on its way to becoming nearly vertical by day 8 (Fig. 8d).

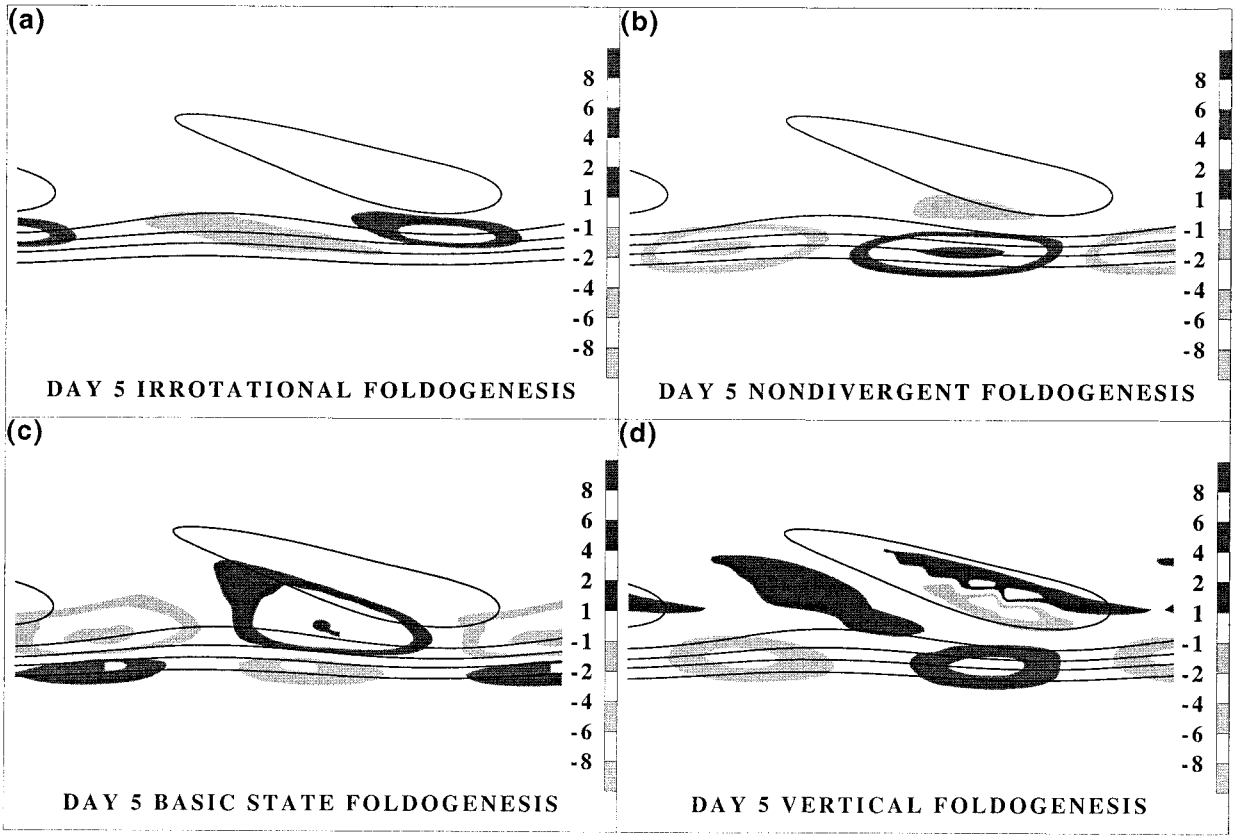

FIG. 10. Day 5 tropopause height z_T (contours and domain as in Fig. 9a) and the (a) irrotational, (b) nondivergent, (c) basic-state, and (d) vertical foldogenesis functions. Shading intervals are indicated in the panels.

b. Day 7

Comparison of the flow fields between days 5 and 7 show that 48 h of evolution have altered little aside from wind speeds. The irrotational wind field (Fig. 12a) remains dominated by the pattern of divergence in the ridge and convergence in the trough. The circulations around the upper-level ridge and trough still dominate the nondivergent wind field (Fig. 12b), though the cyclonic winds in the trough have become stronger than the anticyclonic winds in the ridge. The basic-state wind (Fig. 12c) still has a large along-tropopause component, but the increased amplitude of the wave has increased the flow normal to the tropopause. The wave-relative total wind field (Fig. 12d) shows the fold to be oriented with the confluent streamline. Indeed, the confluent streamline helps determine the location of the fold throughout its development, not only during its initial formation (refer to discussion of Fig. 11d above).

1) FOLDOGENESIS NEAR THE NORTHWESTERLY FLOW INFLECTION POINT

The accelerated development of the fold in the vicinity of the northwesterly flow inflection point at day 7 is due to increased horizontal foldogenesis. The strength of the horizontal terms relative to the vertical term increases greatly between day 5 and day 7 (Figs. 10 and 13; note the change in scale). As mentioned above, the structure of the wind field has changed little over the period, but the increased variation of the height of the tropopause results in an increased contribution by the horizontal winds. The basic-state wind, by definition, is constant in time, but the change in the position and slope of the tropopause leads to changes in the tropopause basic state wind (Figs. 11c and 12c). Horizontal and vertical shears of the horizontal winds exist at day 5, particularly in the basic-state and irrotational wind fields, but the tropopause is nearly flat (Fig. 8a) and thus those winds can have little influence on the orientation of the tropopause. The more strongly sloped tropopause on day 7 (Fig. 8c), however, is configured such that it is susceptible to the effect of the strong vertical shear. Once the vertical motions produce a sufficiently sloped tropopause, the horizontal winds can work to generate the fold (Figs. 12a–c and 13a–c), as discussed in section 3b. The strongest contribution to the foldogenesis in the vicinity of the northwesterly flow inflection point at day 7 is from the vertical shear of the basic-state wind (Figs. 12c and 13c).

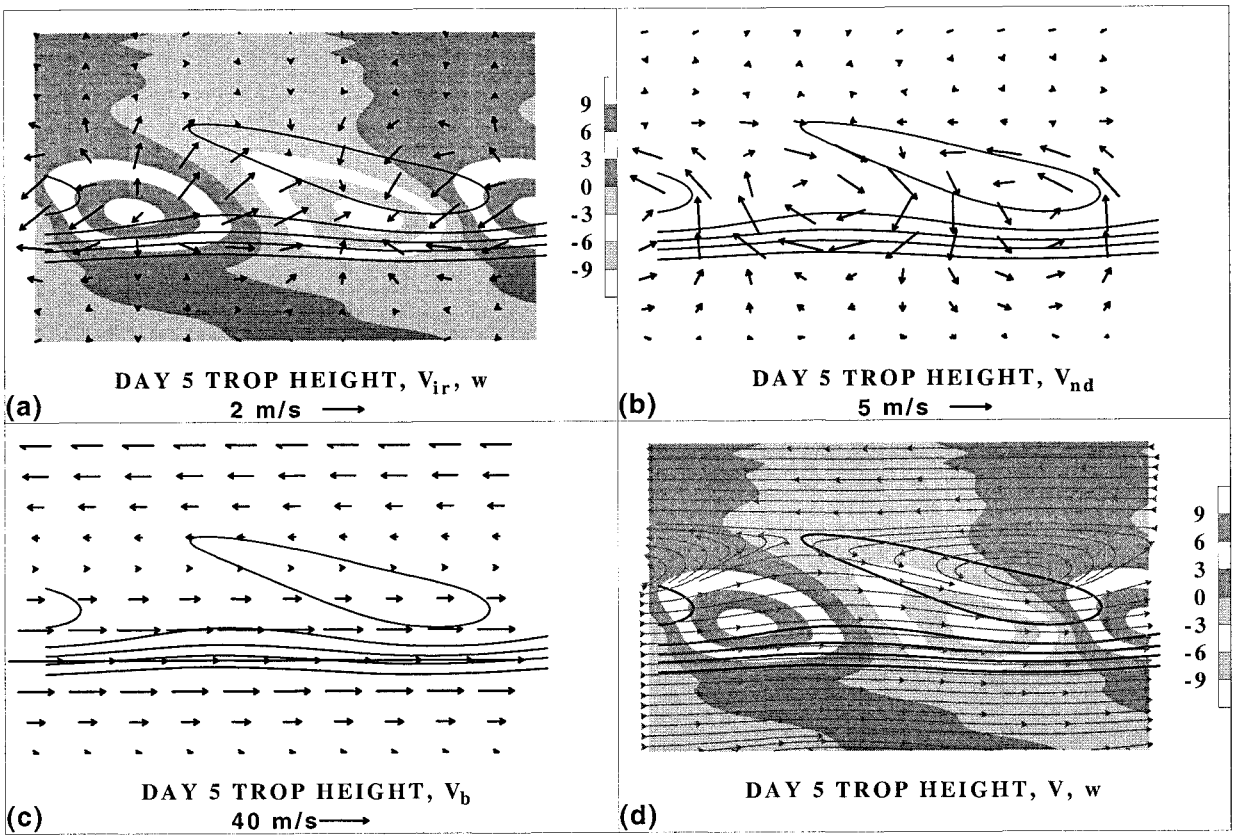

FIG. 11. Day 5 tropopause height z_T (contours and domain as in Fig. 9a) and winds **v** on the tropopause: (a) irrotational $\mathbf{v}_{ir}$ and vertical (shaded), (b) nondivergent $\mathbf{v}_{nd}$, (c) wave-relative basic state $\mathbf{v}_b$, and (d) streamlines of wave-relative total **v** and vertical (shaded). Vector scales are plotted in (a)–(c). Shading intervals (10^{-3} m s^{-1}) are plotted in (a) and (d).

2) FOLDOGENESIS IN THE BASE OF THE TROUGH

The fold in the base of the trough follows a different evolution from the fold near the inflection point. Because a steep tropopause is present in the basic state (Fig. 8a), the horizontal terms need not wait for the vertical motions to take effect to begin contributing foldogenetically, as can be seen by day 5 (Figs. 10a–c). Furthermore, as the slope of the tropopause increases, the vertical motion becomes less effective in changing the slope. Hence, with a nearly vertical tropopause in the base of the trough at day 7, the vertical term contributes relatively little to the total foldogenesis (cf. Fig. 13d with Fig. 9c).

Foldogenesis by the basic-state wind (Fig. 13c) produces a strong dipole centered on the trough. Hints of a similar dipole pattern are found in the other foldogenesis terms as well. This dipole pattern reflects the maintenance rather than the genesis of the tropopause fold. Consistent with the prominent dipole pattern of total (Lagrangian) foldogenesis at day 7 (Fig. 9c), air parcels flowing through the wave experience an increase of tropopause slope as they enter the fold and a very rapid flattening upon exiting, with a residence time within the fold of roughly 12 h.

c. Piecewise partitioning

To understand the foldogenetic contribution of the nondivergent wind it is useful to employ another tool of PV diagnostics: the piecewise partitioning technique described in section 3c. This partitioning uses QGPV inversion and thus approximates the full nondivergent wind by the geostrophic wind. Returning to day 5, when the patterns are simpler, Fig. 14 shows the foldogenesis due to the upper and lower geostrophic winds and plots of those winds on the tropopause. The upper geopotential height wave is nearly in phase with the PV wave, as indicated by the cyclonic circulation near the trough (Fig. 14c). Consequently, the upper nondivergent wind flows mostly along the steep tropopause in the base of the trough, while the cross-tropopause flow is mainly on either side of the trough. Accordingly, the upper nondivergent wind produces a dipole of foldogenesis on either side of the trough (Fig. 14a), with relatively weak net foldogenesis of indeterminate sign as air parcels move through the wave.

The contribution from the lower nondivergent wind is nearly symmetric and concentrated near the trough and ridge axes (Fig. 14b). As expected for the most unstable mode, there is a westward tilt with height of

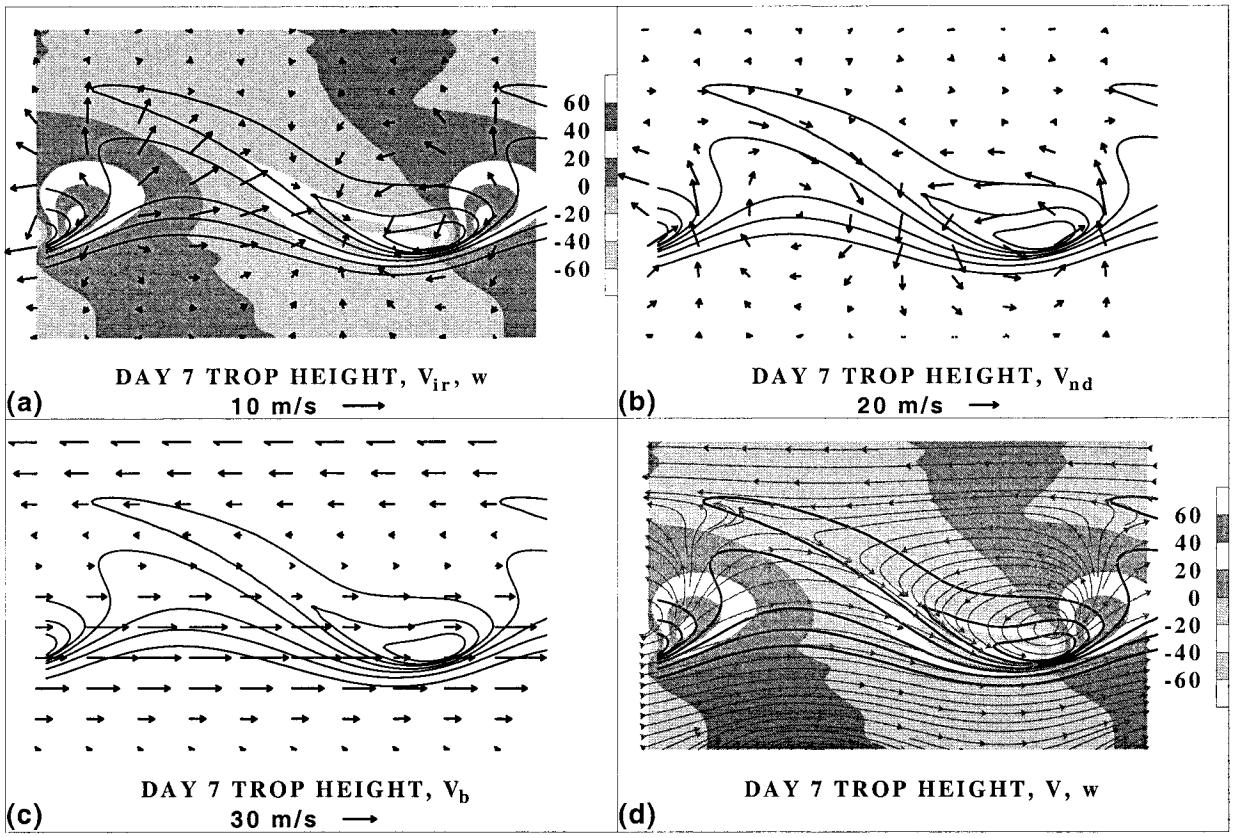

FIG. 12. As in Fig. 11, but for day 7. Shading intervals and vector scales are indicated in the panels.

the growing wave, and in this case the lower wave is nearly 90° out of phase with the upper wave. This eastward shift of the lower wave results in strong northerly flow in the trough (Fig. 14d). Since these winds are associated with the surface cyclone, they are strongest near the surface and decrease in speed with height, yielding a foldogenetic vertical shear. In effect, the lowest part of the tropopause is drawn southward by the circulation associated with the surface cyclone. This process should be common to any upshear tilted baroclinic wave. The foldolysis in the ridge is comparatively weak relative to the foldogenesis in the trough (Fig. 14b). This asymmetry arises because the tropopause slope is weaker in the ridge and because the most steeply sloped region is higher in the ridge than in the trough, so that the lower nondivergent winds on the tropopause are weaker in the most steeply sloped region in the ridge than in the comparable region in the trough (Fig. 14d). As a result of this asymmetry, there is an overall net foldogenetic contribution along the length of the PV wave from the lower nondivergent winds.

As with the other wind components, the partitioned upper and lower nondivergent wind fields show the same patterns at day 7 as at day 5. The upper nondivergent winds (Fig. 15c) flowing through the base of the trough are still associated with a dipole pattern of foldogenesis (Fig. 15a). Meanwhile, foldogenesis in the trough due to the lower nondivergent wind has increased dramatically since day 5 (Figs. 14b and 15b). Not only has the lower nondivergent wind increased with the strengthening of the surface cyclone (Figs. 14d and 15d), but as the tropopause sinks lower, nearer to the cyclone, the vertical shear it encounters gets stronger, bringing the lower portion of the tropopause southward underneath the higher region of the tropopause. With the differences between the ridge and the trough in the strength of the slope and the height of the most strongly sloped region of the tropopause even greater than at day 5, the asymmetry in the foldogenesis pattern increases so that the foldolysis in the ridge is not even of the same order of magnitude as the foldogenesis in the trough. The folding induced by the surface cyclone is even greater on day 8 (not shown), as the vertical motion field draws the fold closer to the surface. Thus, the net effect of the lower nondivergent wind throughout the development of the cyclone consists of the generation and amplification of the tropopause fold in the base of the trough.

d. Day 8

A true tropopause fold ultimately develops between days 7 and 8 (Figs. 8c,d). The formation of the fold

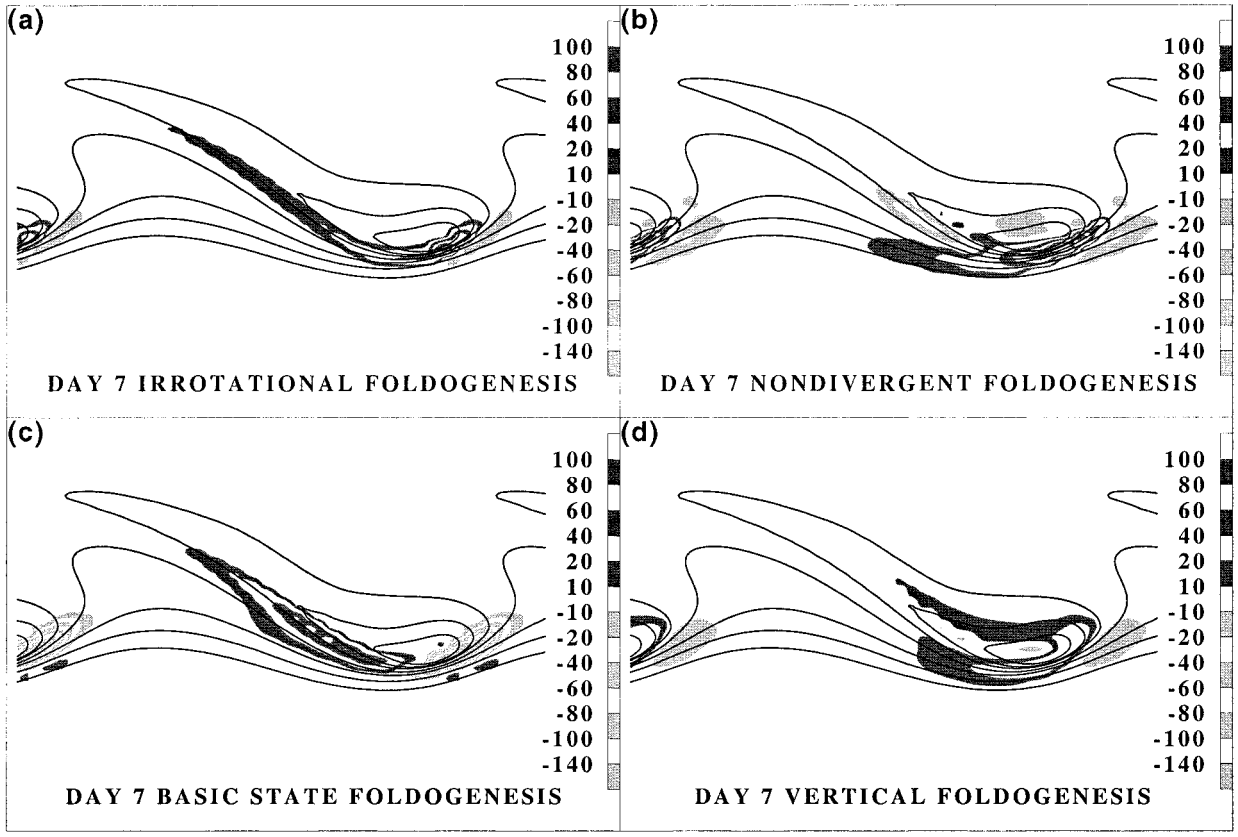

FIG. 13. As in Fig. 10, but for day 7. Shading intervals are indicated in the panels.

represents a continuation of processes that have been active since the quasi-linear growth stage. At day 8, the irrotational (Fig. 16a) and basic-state (Fig. 16c) winds contribute roughly equally near and upstream of the inflection point in the northwesterly flow, while the nondivergent wind (Fig. 16b) amplifies the fold in the base of the trough due to the effect of the winds associated with the low-level cyclone (not shown). Foldogenesis due to vertical motions ceases to be of the same magnitude as horizontal foldogenesis once the tropopause becomes vertical. At this time, intensification of the fold is brought about kinematically through the transport by horizontal winds of stratospheric air underneath upper-level tropospheric air. As the fold intensifies, vertical motion plays the indirect role of driving the stratospheric air even lower into the troposphere, allowing it to experience an ever-greater amount of vertical wind shear.

5. Summary

We have proposed an alternative approach for investigating upper-level frontogenesis using quasigeostrophic potential vorticity (QGPV). The flow was decomposed into vertical and horizontal parts, with further decomposition of the horizontal flow into irrotational and nondivergent components using the technique described by Keyser et al. (1989, 1992). Through piecewise partitioning of the QGPV field, the nondivergent geostrophic wind is split into lower and upper components, associated with lower- and upper-level PV anomalies, respectively. From a two-dimensional plot of these winds on the tropopause surface, the full three-dimensional development can be understood. In this alternative framework, it is more appropriate to focus on tropopause folding instead of frontogenesis. Therefore, rather than examining the differential advection of isentropes to form a tight gradient of potential temperature on a level surface—a front—we focused attention on the differential advection of the tropopause to produce a tight gradient in the tropopause height field: a steepening tropopause. With the aid of this method, it was possible to assess the roles of the various wind components in the evolution of a fold that formed in the course of baroclinic wave development in the channel model used by Rotunno et al. (1994).

The region of the fold that forms in the northwesterly flow between the trough and upstream ridge coincides with an area of cold advection and confluence (Fig. 1). In the traditional perspective, where the emphasis is on the vertical motion field, cold advection and confluence are necessary to force subsidence in the developing fold.

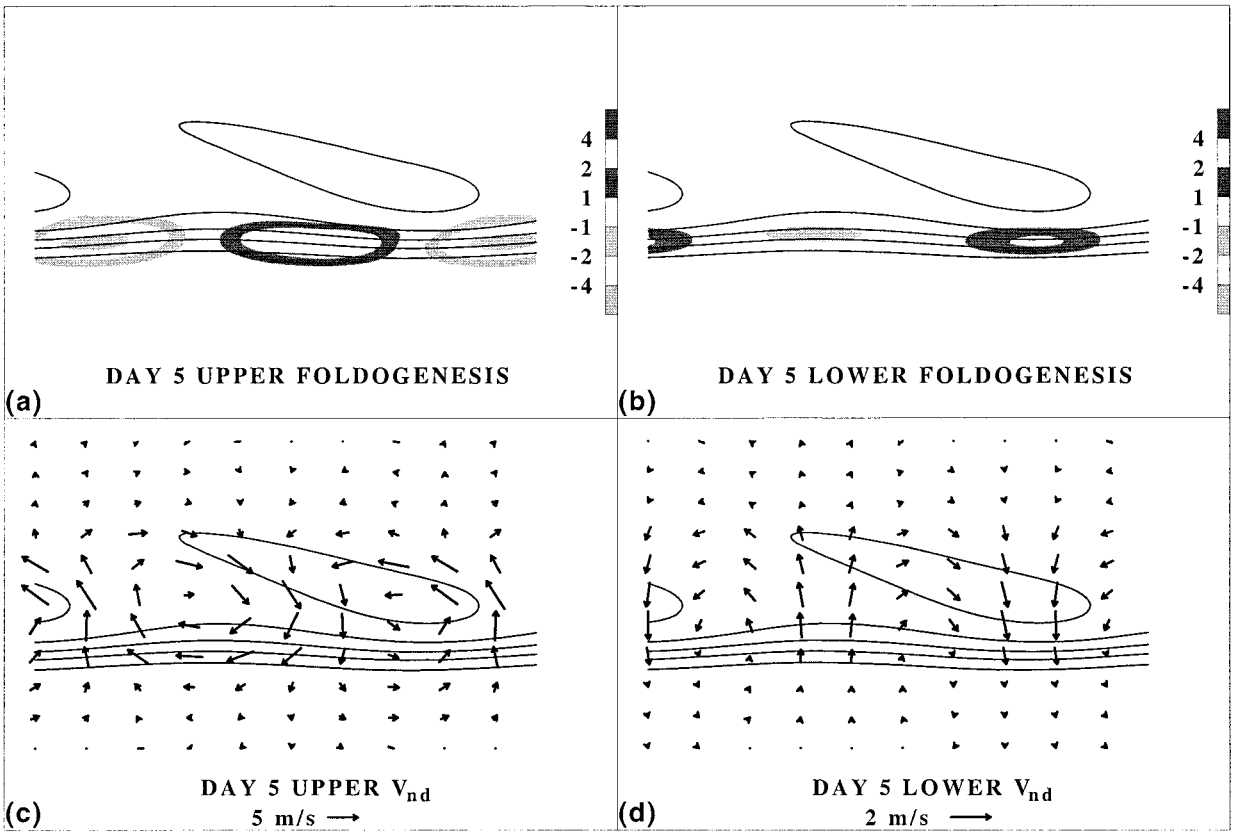

FIG. 14. (a) and (b) As in Fig. 10, but for the upper and lower perturbation nondivergent foldogenesis function, respectively. (c) and (d) As in Fig. 11b, but for the upper and lower perturbation nondivergent wind. Shading intervals and vector scales are indicated in the panels.

In PV thinking, cold advection implies that there exists a vertical shear consistent with thermal wind balance. This vertical shear in the basic-state wind field is foldogenetic and capable of producing a fold by itself. The irrotational flow assists in generating the fold, but it does so along most of the length of the fold and thus is not exclusively tied to cold advection. The vertical motion is important only insofar as it rotates the tropopause out of the horizontal. Once the vertical motion produces a gradient in tropopause height with a component parallel to the vertical shear, the shear is the dominant factor in steepening the slope of the tropopause and in producing a fold.

A crucial factor in the fold evolution is the confluent streamline, which determines the orientation of the fold within the wave. Although the basic state included a steeply sloped tropopause, the upstream fold developed along an initially flat region of the tropopause. The different histories of rising and sinking air parcels on either side of the confluent streamline have the same effect as if a strong gradient of the vertical motion field existed across this streamline. The differential vertical motion experienced by air parcels over the course of several days produces a significantly sloped tropopause along the confluent streamline. The spatial variation in tropopause height exposes the tropopause to the vertical shear of the horizontal wind, which acts to further steepen the tropopause, eventually leading to a fold. R. Rotunno (1999, personal communication) has pointed out to us that the propensity of a fold to form between the trough and upstream ridge during cyclogenesis is likely to depend on the cyclonic or anticyclonic nature of the baroclinic life cycle (see, e.g., Hines and Mechoso 1991; Thorncroft et al. 1993). Our results suggest an alternative interpretation: the confluent streamline, which we identify as the locus for growth of the tropopause slope, would be oriented northwest–southeast even in the absence of horizontal wave tilt or basic-state horizontal shear.

The fold in the base of the trough forms along the basic-state tropopause slope. Because the tropopause there is steeply sloped from the start, the contribution from the differential vertical motion is relatively minor despite the proximity of the sinking maximum. Furthermore, the horizontal winds are able to contribute foldogenetically in the trough base long before they do near the northwesterly flow inflection point. Consequently, the fold forms first, and the horizontal extent

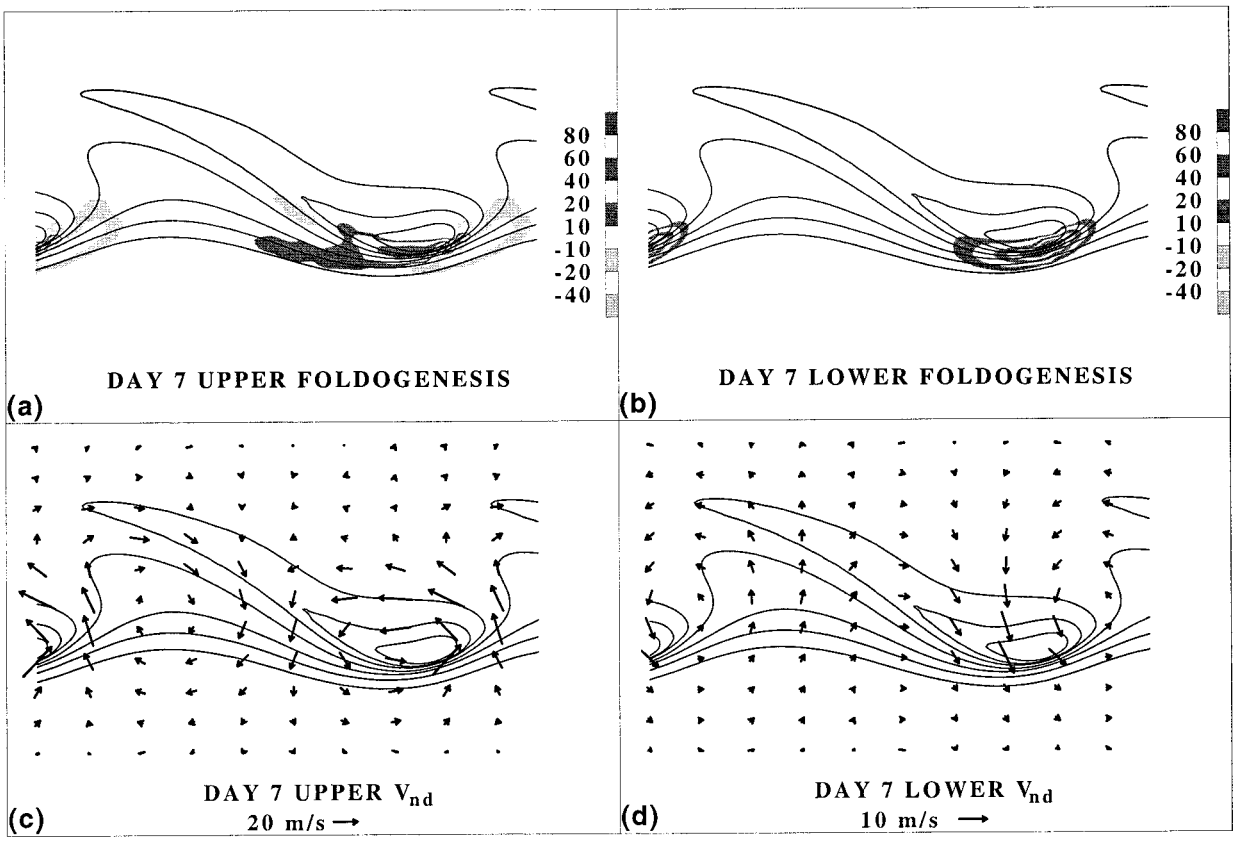

FIG. 15. As in Fig. 14, but for day 7. Shading intervals and vector scales are indicated in the panels.

remains largest, in the trough base. The folding there is due mainly to the winds associated with the developing surface cyclone. As expected in a case of baroclinic normal-mode growth, the lower geopotential height wave is shifted with respect to the upper geopotential height wave, the latter of which is only slightly out of phase with the PV wave. Thus, the steep tropopause in the base of the trough is roughly normal to the strong northerly branch of the low-level circulation. Since the magnitudes of these low-level winds diminish with height, there exists a strong vertical shear to these northerlies that acts to pull the tropopause southward underneath itself, producing the fold (Fig. 17).

In the conventional view of frontogenesis in the base of the trough, described by RSS and others, tilting frontogenesis, associated with a particular vertical motion pattern and forcing configuration, leads to the formation of the upper-level front and to tropopause folding. In the viewpoint espoused here, the folding is a direct consequence of the upshear tilt of the growing baroclinic wave, and the vertical motion pattern plays only a supporting role by maintaining dynamical balance with respect to the evolving PV distribution. Since all growing baroclinic waves tilt with height, this tropopause folding mechanism should be a general characteristic of intensifying extratropical cyclones.

The foldogenetical processes are remarkably similar throughout the evolution of the wave (cf. Figs. 10 and 13). The processes that lead to the fold on day 8 are working to tighten the tropopause height gradient three days earlier (Fig. 10) both in the trough and upstream toward the ridge. The shift in dominance from the vertical to the horizontal terms near the inflection point results from the change in tropopause orientation, which rotates from a flat to an increasingly sloped surface. Otherwise, changes in the foldogenetical function throughout the wave development are limited to strengthening and focusing of this function in select regions as the PV anomalies amplify and the tropopause height gradient intensifies.

To summarize, the tropopause fold that forms in the course of baroclinic wave development is the result of two distinct processes that are consistent throughout the development. Cold advection in the northwesterly flow between the ridge and downstream trough coincides with an area in which tropopause folding is expected from traditional considerations. However, PV diagnostics shift the emphasis from the vertical motion forced by this flow regime to the vertical shear implied by cold advection. The contribution of the basic-state wind, which is nondivergent, is at least as significant in this region as that of the irrotational flow to which tropo-

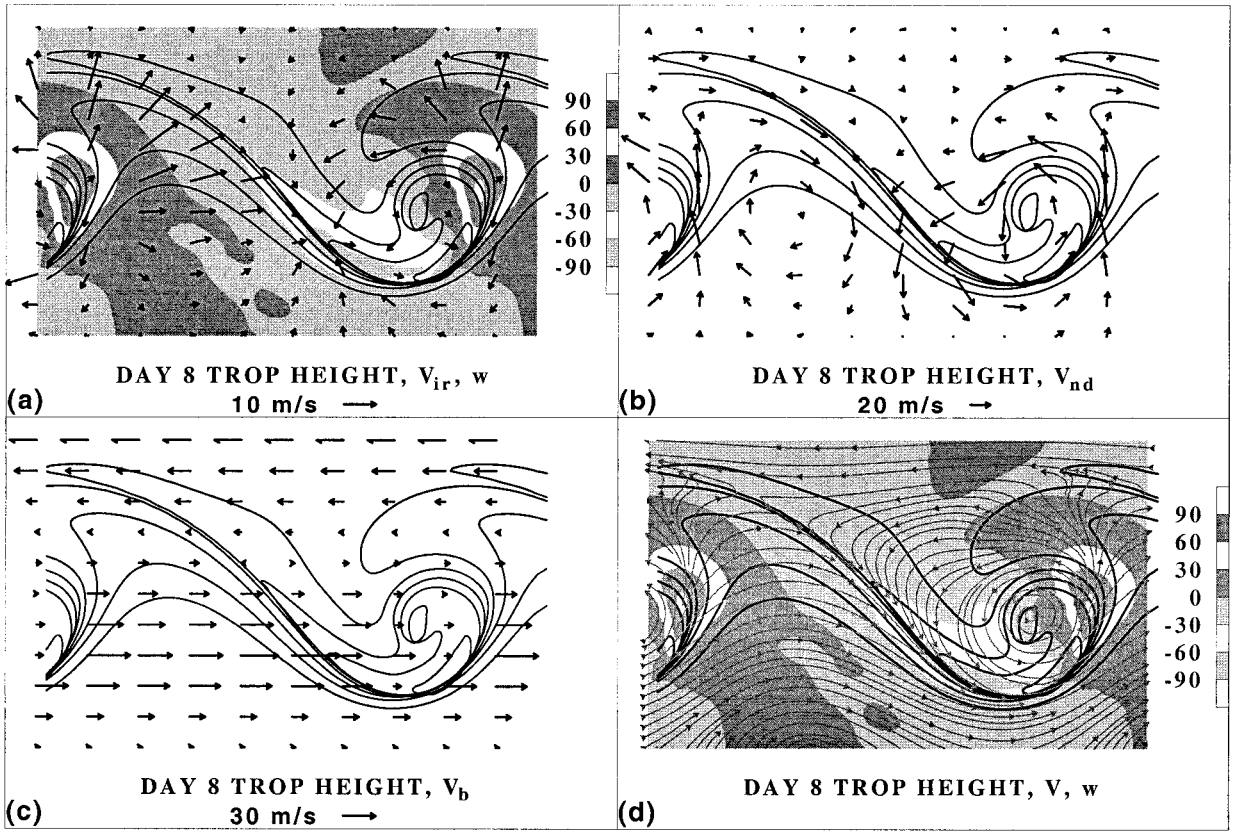

FIG. 16. As in Fig. 11, but for day 8. Shading intervals and vector scales are indicated in the panels.

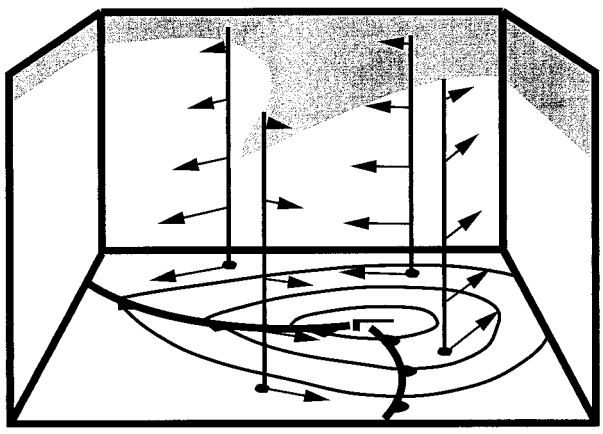

FIG. 17. Perspective view of idealized surface cyclone, seen from the east. Selected profiles show winds associated with the surface thermal wave. (Winds associated with the upper-level trough are not shown.) The shading indicates the location of stratospheric air along the walls of the box. West of the surface cyclone, midlevel northerlies associated with the surface thermal wave advect stratospheric air southward, generating a tropopause fold in the base of the upper-level trough.

pause folding is generally attributed. The location where the fold will form within this region of cold advection is determined by the confluent streamline. The nondivergent flow is responsible for producing the fold in the base of the trough as well, but here the fold is due to the nondivergent wind associated with the surface cyclone. The role of the vertical motion is to increase the exposure of the tropopause to the vertical shear of the nondivergent flow associated with the surface cyclone by increasing the downward penetration of the tropopause fold. While some previous studies have demonstrated that pronounced tropopause folding may precede and initiate intense surface cyclogenesis, the present study shows that tropopause folding may result from the development of a surface cyclone.

Acknowledgments. The authors would like to thank Chris Davis for helping to develop the foldogenesis concept. We also are grateful to Richard Rotunno for lending us the model code and to Louis Wicker and William Skamarock for their assistance with the code. M. Wandishin and J. Nielsen-Gammon were supported by NSF Grants ATM-9553284 and ATM-9521383, and D. Keyser was supported by NSF Grants ATM-9421678 and ATM-9818088.

REFERENCES

Bluestein, H. B., 1993: *Synoptic-Dynamic Meteorology in Midlatitudes.* Vol. 2, *Observations and Theory of Weather Systems,* Oxford University Press, 594 pp.

Bosart, L. F., 1970: Mid-tropospheric frontogenesis. *Quart. J. Roy. Meteor. Soc.,* **96,** 442–471.

Bush, A. B. G., and W. R. Peltier, 1994: Tropopause folds and synoptic-scale baroclinic wave life cycles. *J. Atmos. Sci.,* **51,** 1581–1604.

Cammas, J.-P., and D. Ramond, 1989: Analysis and diagnosis of the composition of ageostrophic circulations in jet-front systems. *Mon. Wea. Rev.,* **117,** 2447–2462.

Davies, H. C., and A. M. Rossa, 1998: PV frontogenesis and upper-tropospheric fronts. *Mon. Wea. Rev.,* **126,** 1528–1539.

Davis, C. A., 1992: Piecewise potential vorticity inversion. *J. Atmos. Sci.,* **49,** 1397–1411.

——, and K. A. Emanuel, 1991: Potential vorticity diagnostics of cyclogenesis. *Mon. Wea. Rev.,* **119,** 1929–1953.

——, M. T. Stoelinga, and Y.-H. Kuo, 1993: The integrated effect of condensation in numerical simulations of extratropical cyclogenesis. *Mon. Wea. Rev.,* **121,** 2309–2330.

——, E. D. Grell, and M. A. Shapiro, 1996: The balanced dynamical nature of a rapidly intensifying oceanic cyclone. *Mon. Wea. Rev.,* **124,** 3–26.

Hakim, G. J., D. Keyser, and L. F. Bosart, 1996: The Ohio Valley wave-merger cyclogenesis event of 25–26 January 1978. Part II: Diagnosis using quasigeostrophic potential vorticity inversion. *Mon. Wea. Rev.,* **124,** 2176–2205.

Hines, K. M., and C. R. Mechoso, 1991: Frontogenesis processes in the middle and upper troposphere. *Mon. Wea. Rev.,* **119,** 1225–1241.

Hoerling, M. P., T. D. Schaack, and A. J. Lenzen, 1991: Global objective tropopause analysis. *Mon. Wea. Rev.,* **119,** 1816–1831.

Hoskins, B. J., 1971: Atmospheric frontogenesis models: Some solutions. *Quart. J. Roy. Meteor. Soc.,* **97,** 139–153.

——, 1972: Non-Boussinesq effects and further development in a model of upper tropospheric frontogenesis. *Quart. J. Roy. Meteor. Soc.,* **98,** 532–541.

——, 1982: The mathematical theory of frontogenesis. *Annu. Rev. Fluid Mech.,* **14,** 131–151.

——, and F. P. Bretherton, 1972: Atmospheric frontogenesis models: Mathematical formulation and solution. *J. Atmos. Sci.,* **29,** 11–37.

——, M. E. McIntyre, and A. W. Robertson, 1985: On the use and significance of isentropic potential vorticity maps. *Quart. J. Roy. Meteor. Soc.,* **111,** 877–946.

Juckes, M., 1999: The structure of idealized upper-tropospheric shear lines. *J. Atmos. Sci.,* **56,** 2830–2845.

Keyser, D., 1999: On the representation and diagnosis of frontal circulations in two and three dimensions. *The Life Cycles of Extratropical Cyclones,* M. A. Shapiro and S. Grønås, Eds., Amer. Meteor. Soc., 239–264.

——, and M. J. Pecnick, 1985: A two-dimensional primitive equation model of frontogenesis forced by confluence and horizontal shear. *J. Atmos. Sci.,* **42,** 1259–1282.

——, and M. A. Shapiro, 1986: A review of the structure and dynamics of upper-level frontal zones. *Mon. Wea. Rev.,* **114,** 452–499.

——, B. D. Schmidt, and D. G. Duffy, 1989: A technique for representing three-dimensional vertical circulations in baroclinic disturbance. *Mon. Wea. Rev.,* **117,** 2463–2494.

——, ——, and ——, 1992: Quasigeostrophic diagnosis of three-dimensional ageostrophic circulations in an idealized baroclinic disturbance. *Mon. Wea. Rev.,* **120,** 698–730.

Lackmann, G. M., D. Keyser, and L. F. Bosart, 1997: A characteristic life cycle of upper-tropospheric cyclogenetic precursors during the Experiment on Rapidly Intensifying Cyclones over the Atlantic (ERICA). *Mon. Wea. Rev.,* **125,** 2729–2758.

Lamarque, J.-F., and P. G. Hess, 1994: Cross-tropopause mass exchange and potential vorticity budget in a simulated tropopause folding. *J. Atmos. Sci.,* **51,** 2246–2269.

Loughe, A. F., C.-C. Lai, and D. Keyser, 1995: A technique for diagnosing three-dimensional ageostrophic circulations in baroclinic disturbances on limited-area domains. *Mon. Wea. Rev.,* **123,** 1476–1504.

Morgan, M. C., 1999: Using piecewise potential vorticity inversion to diagnose frontogenesis. Part I: A partitioning of the Q vector applied to diagnosing surface frontogenesis and vertical motion. *Mon. Wea. Rev.,* **127,** 2796–2821.

——, and J. W. Nielsen-Gammon, 1998: Using tropopause maps to diagnose midlatitude weather systems. *Mon Wea. Rev.,* **126,** 2555–2579.

Namias, J., and P. F. Clapp, 1949: Confluence theory of the high tropospheric jet stream. *J. Meteor.,* **6,** 330–336.

Newton, C. W., and A. Trevisan, 1984: Clinogenesis and frontogenesis in jet-stream waves. Part I: Analytic relations to wave structure. *J. Atmos. Sci.,* **41,** 2717–2734.

Nielsen-Gammon, J. W., and R. J. Lefevre, 1996: Piecewise tendency diagnosis of dynamical processes governing the development of an upper-tropospheric mobile trough. *J. Amos. Sci.,* **53,** 3120–3142.

Petterssen, S., 1956: *Weather Analysis and Forecasting.* Vol. 1, *Motion and Motion Systems,* 2d ed., McGraw-Hill, 428 pp.

Reed, R. J., 1955: A study of a characteristic type of upper-level frontogenesis. *J. Meteor.,* **12,** 226–237.

——, and F. Sanders, 1953: An investigation of the development of a mid-tropospheric frontal zone and its associated vorticity field. *J. Meteor.,* **10,** 338–349.

Reeder, M. J., and D. Keyser, 1988: Balanced and unbalanced upper-level frontogenesis. *J. Atmos. Sci.,* **45,** 3366–3386.

Rotunno, R., W. C. Skamarock, and C. Snyder, 1994: An analysis of frontogenesis in numerical simulations of baroclinic waves. *J. Atmos. Sci.,* **51,** 3373–3398.

Sanders, F., L. F. Bosart, and C.-C. Lai, 1991: Initiation and evolution of an intense upper-level front. *Mon. Wea. Rev.,* **119,** 1337–1367.

Shapiro, M. A., 1970: On the applicability of the geostrophic approximation to upper-level frontal-scale motions. *J. Atmos. Sci.,* **27,** 408–420.

——, 1981: Frontogenesis and geostrophically forced secondary circulations in the vicinity of jet stream-frontal zone systems. *J. Atmos. Sci.,* **38,** 954–973.

Staley, D. O., 1960: Evaluation of potential-vorticity changes near the tropopause and the related vertical motions, vertical advection of vorticity, and transfer of radioactive debris from stratosphere to troposphere. *J. Meteor.,* **17,** 591–620.

Thorncroft, C. D., B. J. Hoskins, and M. E. McIntyre, 1993: Two paradigms of baroclinic-wave life-cycle behaviour. *Quart. J. Roy. Meteor. Soc.,* **119,** 17–55.

Uccellini, L. W., and P. J. Kocin, 1987: The interaction of jet streak circulations during heavy snow events along the East Coast of the United States. *Wea. Forecasting,* **2,** 289–308.

——, D. Keyser, K. F. Brill, and C. H. Wash, 1985: The Presidents' Day cyclone of 18–19 February 1979: Influence of upstream trough amplification and associated tropopause folding on rapid cyclogenesis. *Mon. Wea. Rev.,* **113,** 962–988.

Whitaker, J. S., L. W. Uccellini, and K. F. Brill, 1988: A model-based diagnostic study of the rapid development phase of the Presidents' Day cyclone. *Mon. Wea. Rev.,* **116,** 2337–2365.